hydrology

MDPI

Article

Advancing Coastal Flood Risk Prediction Utilizing a GeoAI Approach by Considering Mangroves as an Eco-DRR Strategy

Tri Atmaja [1,2], Martiwi Diah Setiawati [3,4,*], Kiyo Kurisu [1] and Kensuke Fukushi [1,3]

[1] Department of Urban Engineering, Graduate School of Engineering, The University of Tokyo, Tokyo 113-8654, Japan
[2] Research Center for Climate and Atmosphere, National Research and Innovation Agency (BRIN), Jakarta 10340, Indonesia
[3] Institute for the Advanced Study of Sustainability (UNU-IAS), United Nations University, Tokyo 150-8925, Japan
[4] Research Center for Oceanography, National Research and Innovation Agency (BRIN), Jakarta 10340, Indonesia
* Correspondence: martiwi1802@gmail.com

Abstract: Traditional coastal flood risk prediction often overlooks critical geographic features, underscoring the need for accurate risk prediction in coastal cities to ensure resilience. This study enhances the prediction of coastal flood occurrence by utilizing the Geospatial Artificial Intelligence (GeoAI) approach. This approach employed models—random forest (RF), k-nearest neighbor (kNN), and artificial neural networks (ANN)—and compared them to the IPCC risk framework. This study used El Salvador as a demonstration case. The models incorporated seven input variables: extreme sea level, coastline proximity, elevation, slope, mangrove distance, population, and settlement type. With a recall score of 0.67 and precision of 0.86, the RF model outperformed the other models and the IPCC approach, which could avoid imbalanced datasets and standard scaler issues. The RF model improved the reliability of flood risk assessments by reducing false negatives. Based on the RF model output, scenario analysis predicted a significant increase in flood occurrences by 2100, mainly under RCP8.5 with SSP5. The study also highlights that the continuous mangrove along the coastline will reduce coastal flood occurrences. The GeoAI approach results suggest its potential for coastal flood risk management, emphasizing the need to integrate natural defenses, such as mangroves, for coastal resilience.

Keywords: coastal flood risk; GeoAI; random forest; IPCC risk approach; mangroves; disaster risk management; coastal resilience

Citation: Atmaja, T.; Setiawati, M.D.; Kurisu, K.; Fukushi, K. Advancing Coastal Flood Risk Prediction Utilizing a GeoAI Approach by Considering Mangroves as an Eco-DRR Strategy. *Hydrology* **2024**, *11*, 198. https://doi.org/10.3390/hydrology11120198

Academic Editor: Miklas Scholz

Received: 24 October 2024
Revised: 20 November 2024
Accepted: 21 November 2024
Published: 23 November 2024

1. Introduction

Coastal zones worldwide are increasingly vulnerable to climate-related hazards, with coastal floods emerging as one of the most pressing threats [1]. Coastal flooding refers to seawater penetrating land caused by unpredictable high-water occurrences, such as regular high tides or storm surges resulting from tropical cyclones, storms, or typhoons, lasting at least one day in coastal regions [2]. Climate change is expected to increase the frequency of coastal flooding due to rising sea levels, enhanced storm surges, and changes in precipitation patterns. This danger poses substantial hazards to human populations, infrastructure, and ecosystems in these coastal zones [3,4]. Consequently, comprehending coastal flooding and its related effects is essential.

Previous studies have utilized coastal flood risks to ascertain the potential extent of inundated areas and the anticipated exposed populations or assets [5–7]. Coastal flood risk is the probability of coastal flood occurrence in specific regions, driven by physical and social factors, including hydrometeorological, geophysical, and socio-economic

variables. At the same time, the aggregate of detrimental consequences, income loss, and property damage induced by coastal floods is termed the impact [8]. Prior research employed coastal flood risk prediction to assess flooding likelihood and impact in coastal areas by integrating the abovementioned factors [2,7]. Generally, coastal flood risks are predicted using a statistical approach. This examines flood drivers' correlations and similarities, utilizing historical data and statistical models to identify patterns and relationships, such as regression, probability, or machine learning (ML) models [7,9–11].

Coastal zones are subject to severe coastal flood risk, necessitating the development of more accurate and reliable flood risk prediction methods due to the limitations of current approaches [12,13]. The current approaches in coastal flood prediction often use univariate probability distributions that fail to account for the complex interactions between multiple flood drivers [12,13]. Another significant limitation is the underutilization of geographic features, i.e., proximity, shape, or density. Future coastal risk prediction should elaborate on the proximity of mangrove ecosystems, which function as natural defenses [14–16]. Mangroves have been demonstrated to dissipate wave energy and stabilize shorelines; however, their role is often overlooked in conventional flood risk prediction [17,18]. This omission is particularly critical given the growing recognition of mangroves as ecosystem-based disaster risk reduction (Eco-DRR) strategies, which emphasize integrating natural ecosystems into disaster risk management.

Recent advances in geospatial technologies and artificial intelligence (AI) have offered promising avenues for addressing these gaps. The geospatial artificial intelligence (GeoAI) approach utilizes ML models to elucidate location-based analytics, with a particular focus on the application of spatial (geographic feature) information [19–21]. This technique integrates geospatial science with AI techniques, either ML or deep learning (DL), to analyze and interpret spatial data. GeoAI enables the development of more robust and precise flood risk assessments by handling large and multi-dimensional data [19,20]. By incorporating a more comprehensive range of features, including natural defenses and additional geographical features, GeoAI is anticipated to enhance the robustness of coastal flood risk prediction [19].

This study aims to advance coastal flood risk prediction by employing GeoAI approaches, specifically utilizing random forest (RF), k-nearest neighbor (kNN), and artificial neural network (ANN) models, which are among the most commonly used models [22,23]. This study compares these models with the conventional Intergovernmental Panel on Climate Change (IPCC) risk assessment concept to demonstrate GeoAI's potential in reliably predicting coastal flood occurrences. The framework was applied to coastal hazard-prone areas, focusing on low- to lower-middle-income countries (LLMIC) and utilizing El Salvador as a case study for demonstration purposes. Seven key forcing variables—extreme sea level (ESL), coastline proximity, elevation, slope, mangrove distance, population, and settlement type—were incorporated into the GeoAI models to predict coastal flood occurrences as the target variable.

The significance of this study lies in its potential to address the disparity between conventional risk assessments and the necessity for more comprehensive, data-driven methodologies that incorporate geographical features and mangroves as natural barriers into predictive models. By elucidating the role of mangroves and other geographic elements in mitigating flood risks, this research contributes to the growing body of literature advocating for Eco-DRR strategies. These findings are anticipated to inform more effective risk management practices, ultimately enhancing the resilience of coastal communities to climate change.

2. Materials and Methods

2.1. Development of Coastal Flood Pathways and Key Variables

The study developed and identified coastal flood pathways, and the key variables used to feed the GeoAI model input in predicting coastal flood occurrences as a target. This process was achieved through (i) a literature review and (ii) a structured data collection process. First, a comprehensive review of the existing literature was conducted to analyze and identify the variables used in previous coastal flood risk studies. The review covered publications from all years available in the Web of Science and ScienceDirect databases, focusing on articles featuring case studies in coastal flood risk assessments. The search keyword was "coastal flood risk variables". This review specifically targeted the identification of different variables used in coastal flood risk assessment and the documentation of data sources and formats used. The outcome of this review yielded a list of key forcing variables, which subsequently guided the data collection and risk simulation processes.

The subsequent step involved a data collection process that entailed archiving geophysical, socioeconomic, hydrometeorological, and other relevant datasets that were recently available, accessible, and freely usable for academic purposes. These global datasets, documented extensively in prior research [24], were critical for building the simulation model. We paid particular attention to the spatial and temporal resolution of the data sources to ensure their adequate capture of relevant features and the variability of key variables over time. The GeoAI approach integrates and analyzes extensive datasets from various sources by leveraging big data to generate robust and reliable coastal flood pathways and key variables.

Based on the literature review and extensive data collection, this study identified seven key variables and pathways contributing to coastal flood risk adopted from previous studies [25–32]. These variables encompass ESL, coastline proximity, elevation, slope, mangrove distance, population, and settlement types, as shown in the Supplementary Material, Table S1. Coastal flood occurrence is defined as the penetration of seawater onto land due to storm tides and surges that persist for a duration of one day. ESL represents areas anticipated to be inundated by ESL. Coastline proximity refers to the accumulated distance for each grid within the study boundary to the coastline, calculated using Euclidean distance. Elevation is the topographic height above sea level, while slope indicates the percent change in elevation over a specific distance for each grid. Mangrove distance measures the accumulated distance from each grid within the boundary to mangrove areas, estimated via Euclidean distance. Population represents the number of individuals per grid, and settlement types categorize the nature of settlements based on population density. These variables were utilized to inform the GeoAI model in predicting coastal flood occurrences as the target variable. A detailed description, sources, and data specifications are provided in Table 1.

It should be noted that wave variables were omitted from this study. The interaction between waves and tides can modulate nearshore wave heights, increasing the risk of flooding during high water levels [33,34]. Wave overtopping, driven by stochastic wave behavior, can lead to significant coastal flooding [35,36]. However, the randomness of waves introduces uncertainties in flood projections, especially on short time scales [35,36]. Additionally, given the study's focus on geomorphological and land-based flood drivers, the decision was made to exclude wave variables from the coastal flood risk prediction in this study. Therefore, considering the limitations inherent in current coastal flood risk prediction methodologies, future research efforts should prioritize incorporating wave action, particularly infragravity waves. Infragravity waves, which are long-period waves generated by the interaction of shorter wind waves with the ocean floor and coastal topography, can significantly influence coastal hydrodynamics and sediment transport processes, even in shallow mangrove areas [37,38]. Additionally, Vousdoukas et al. (2016) highlighted that excluding wave contributions in Total Water Level (TWL) estimations

could result in approximately a 60% underestimation of flooded areas [39]. Their inclusion in flood risk assessments could enhance the accuracy and reliability of predictions regarding coastal inundation and erosion [37].

Table 1. Description and profile of the key variables.

Key Variable	Raw Data Format	Original Horizontal Resolution	Temporal Resolution	Raw Data and URL Sources	Variable Profile
Coastal flood occurrence	GeoTIFF	250 m	2000–2018	Ref. [40], Global Flood Database, https://global-flood-database.cloudtostreet.ai (accessed on 10 December 2021)	1: flood 0: no flood
Extreme Sea Level (ESL)	Point	NA	1980–2100	Ref. [39], European Commission, http://data.europa.eu/89h/jrc-liscoast-10012 (accessed on 9 August 2021)	meter ESL
Coastline proximity	Line	NA	2000	Author, based on Prototype Global Shoreline Data, https://shoreline.noaa.gov/data/datasheets/pgs.html (accessed on 17 September 2021)	Index
Elevation	GeoTIFF	90 m	2020	Ref. [41], CoastalDEM Database, https://go.climatecentral.org/coastaldem (accessed on 17 September 2021)	m asl
Slope	GeoTIFF	90 m	2020	Ref. [41], CoastalDEM Database, https://go.climatecentral.org/coastaldem (accessed on 17 September 2021)	%
Mangrove distance	GeoTIFF	30 m	2021	Ref. [42], Global Distribution of Mangroves USGS, https://data.unep-wcmc.org/datasets/4 (accessed on 8 Juni 2021)	Index
Population	GeoTIFF	1 km	2010–2100	Ref. [43], Socioeconomic Data and Applications Center (SEDAC), https://doi.org/10.7927/q7z9-9r69 (accessed on 15 February 2022)	people
Settlement types	GeoTIFF	90 m	2020	Ref. [44], Urban-Rural Catchment Areas (URCAs), https://doi.org/10.1073/pnas.2011990118 (accessed on 25 October 2021)	1 to 10 types

2.2. Development and Evaluation of Coastal Flood Risk Model Utilizing GeoAI Approach

The GeoAI model was developed to predict coastal flood risk occurrences utilizing key variables outlined in Section 2.1. The model was used to predict coastal flood occurrence in three main periods: baseline within 2000–2020 and projections for 2050 and 2100. The coastal flood occurrence in binary format for 2000–2018 served as the target variable (Y), while the key variables functioned as features or independent variables (X). The key variables outlined in Section 2.1 included ESL, coastline proximity, elevation, slope, mangrove distance, population, and settlement types. The coastal flood risk model was constructed in three key stages, as depicted in Figure 1: 2.2.2.) Data Preparation, 2.2.3.) Risk Simulation, and 2.5.) Risk Projection. A detailed description of the demonstration case is provided in Section 2.2.1.) Selection of Case Study.

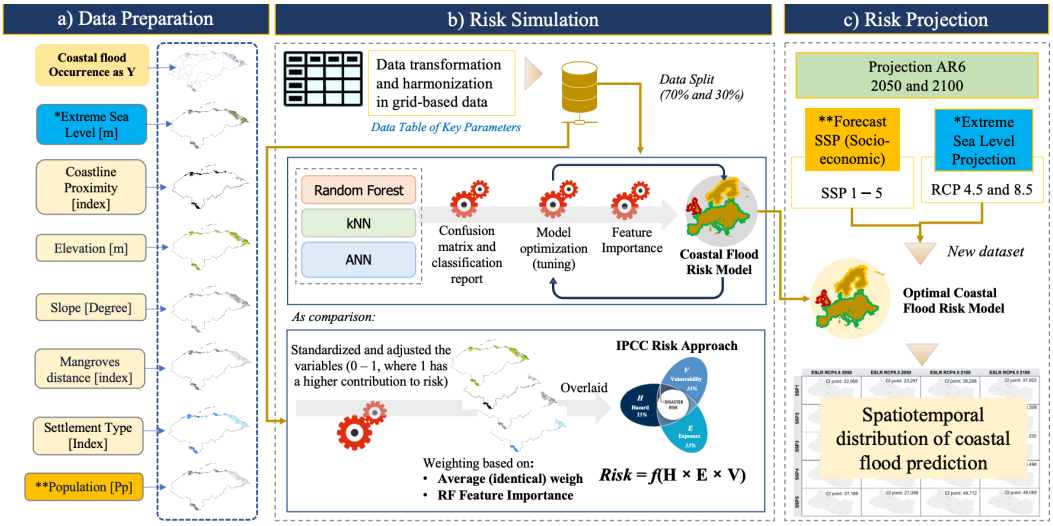

Figure 1. Workflow for coastal flood risk prediction utilizing the GeoAI approach compared to the IPCC risk approach. The data under (*) and (**) indicated that the data had been projected for future ESL and population change following RCP and SSP scenarios, respectively.

2.2.1. Selection of Case Study

The GeoAI model was demonstrated to predict coastal flood occurrences using El Salvador as a case study. Coastal floods in El Salvador are a significant concern due to their location and various natural hazards such as tsunamis, flash floods, and sea swell events. According to historical data, between 2000 and 2018, El Salvador experienced significant coastal flood incidents, resulting in the inundation of over 28 km², affecting approximately 3415 people and impacting settlements over 0.57 km² [40]. Prediction uncertainty increases with basin size in El Salvador's coastal flood basins, highlighting the need for accurate parameter estimation [45].

Moreover, a previous study documented an unprecedented sea swell event in 2015 that substantially impacted the coastline of El Salvador. This occurrence resulted in severe coastal flooding and alterations to the shoreline. The highest levels of erosion and accretion were recorded at 268 m in El Salvador [46]. Analysis of satellite data indicated that El Salvador experienced the most extensive erosion and inundation among several Latin American urban areas examined [46].

Additionally, El Salvador's coastal wetlands, represented by mangrove forests, serve as the primary barrier against flooding and tsunamis, mitigating erosion and coastal floods [47]. The mangrove areas in El Salvador encompassed approximately 38,443 ha in 2011, which represented a 0.32% decrease compared to the areas in 1998 [47]. In terms of ecosystem services, a recent study indicated that losses in ecosystem services provided by mangroves accounted for 9% of the decline in El Salvador, underscoring the severity of further losses [47]. This loss diminishes the mangroves' function as natural barriers against coastal floods.

Given these factors, El Salvador represents an optimal case study for evaluating the GeoAI model's efficacy in predicting coastal flood risks. The country's substantial history of coastal flood events was well-documented, with openly available data extensively provided by the Dartmouth Flood Observatory (DFO). These events were also mapped spatially in the Global Flood Observatory, offering valuable resources for flood risk analysis. Additionally, flood's dependence on mangrove ecosystems for natural flood mitigation provides a comprehensive context for assessing the model's utility. El Salvador's vulnerability, attributable to frequent extreme weather events, exacerbated by socioeconomic challenges and limited resources for conventional flood, underscores the necessity of innovative predictive tools such as GeoAI. Focusing on El Salvador, this study addresses local flood prediction requirements and elucidates the broader applicability of the GeoAI

approach for other similarly vulnerable coastal regions where mangrove conservation is crucial as Eco-DRR.

2.2.2. Data Preparation

The coastal flood risk model utilized the key variables identified in Section 2.1 and illustrated in Figure 1. The data were selected and prepared to capture the primary drivers and modifiers of flood risk. The data for simulation were confined to the research boundary, specifically the Low Elevation Coastal Zone (LECZ), which is considered prone to coastal flooding [4]. It covered all areas with an elevation below 10 m above sea level and hydrologically connected to the coast. The data were prepared using ArcGIS Pro 2.8. Due to the varying spatial resolutions of the datasets, a resampling technique was implemented to harmonize the datasets to a 30 m resolution.

The resampling functions, e.g., nearest neighbor and bilinear, were utilized to handling the data. According to previous study, the optimal resampling method for preserving sharpness and pixel break in high-resolution satellite images is contingent upon the image processing operation, spatial resolution, and evaluation parameters [48]. Previous research has demonstrated that when images are resampled to high spatial resolution, the object statistical features and classification accuracy are minimally affected by object boundary uncertainty; consequently, both raster and vector object boundary transfers are viable approaches [49]. In light of this consideration, we subsequently utilized the nearest neighbor and bilinear methods for resampling our datasets.

The bilinear technique performs a bilinear interpolation and determines the new value of a cell based on a weighted distance average of the four nearest input cell centers. It is suitable for continuous data and results in some smoothing of the data. Yet, we considered the limitation that bilinear interpolation resampling technique had a relative error of 7.2% in streamflow simulations [50]. For example, in hydrological modeling, bilinear interpolation was used to resample elevation, despite it is affecting the accuracy of river network extraction and streamflow simulations [50]. Bilinear interpolation tends to produce more accurate results when resampling continuous data, as it considers the values of surrounding pixels to create a weighted average [51]. The nearest neighbor is a resampling technique that involve selecting the nearest pixel value to estimate new pixel values. This method is suitable used for categorical or ordinal datasets [52]. However, nearest neighbor interpolation can lead to noticeable artifacts such as blockiness and blurriness, which degrade image quality [53]. We acknowledged this limitation and suggested advances method. For instance, sparse neighbor selection and Semi-Nonnegative Matrix Factorization (SNMF) can achieve higher quality super-resolution images compared to traditional nearest neighbor method [54]

Below is a comprehensive description of these variables, their data characteristics, and the interpolation techniques employed. The variables included coastal flood occurrences as the target variable, alongside ESL, coastline proximity, slope, elevation, mangrove distance, population, and settlement types.

- The coastal flood occurrence, serving as the target variable, was defined as a coastal flood event lasting at least one day, as acquired from the Global Flood Database from 2000 to 2018, https://global-flood-database.cloudtostreet.ai (accessed on 10 December 2021). These coastal flood occurrence data were recorded as binary values (1 indicating a flood, 0 indicating no flood) [40] with raster format in 250 m grid size. However, potential biases, such as false positives, were acknowledged in the model-generated data. To harmonize the data into a 30 m grid size, we resampled the aforementioned data using nearest-neighbor techniques, as this pertains to classified (binary) data, and utilized the mask with the elevation as a boundary.
- ESL was identified as a critical variable due to the escalating risk of coastal floods associated with sea-level rise [24]. We used the global ESL projections data by European Commission, gathered from http://data.europa.eu/89h/jrc-liscoast-10012

(accessed on 9 August 2021) [39]. The data, in point format, has presented probabilistic projections of ESL until the end of the 21st century along the global coastline, considering the contributions of mean sea level, tides, waves, and storm surges [39]. These data were utilized due to their recognition of sea level and consideration of its temporal variances, which address the challenges encountered in Copernicus Marine and ECMWF data [55,56]. Copernicus marine operational ocean models can forecast extreme coastal water levels with satisfactory performance but underestimate peak magnitudes by 10% for water levels and 18% for surges [56], while ECMWF, i.e., ORAS5, still underestimates the temporal variance of sea level and continues exhibiting large SST biases in the Gulf Stream and its extension regions [55]. For instance, these European Commission datasets were previous used in the study of worst-case scenarios for ESL [57].

Specifically, we used median values of the ESL data, for period baseline, RCP45-2050, RCP4.5-2100, RCP8.5-2050, and RCP8.5-2100 [39]. The distance of each point is approximately 25 km. We used median values of the ESL data, for period baseline, RCP45-2050, RCP4.5-2100, RCP8.5-2050, and RCP8.5-2100. These data were subsequently mapped spatially and converted into raster format with a 0.54 grid size. A bilinear resampling technique was employed to transform the grid size to 30 m, aligning with previous study [50]. We hypothesized that regions within the same grid exhibit similarities in metocean and atmospheric conditions, as well as in trends of climate extremes. The inland areas with elevations below the ESL were anticipated to be inundated by ESL and were consequently treated as the ESL variable in meter units.

- Coastline proximity is an accumulated distance for each grid within the boundary to the coastline. Prototype Global Shoreline Data, from NOAA, https://shoreline.noaa.gov/data/datasheets/pgs.html (accessed on 17 September 2021), were used to calculate this coastline distance of each cell in 30 m grid size using Euclidean distance considering weight of other cells. The area closer to the coastline is considered more prone to coastal flood risk. These data were shown in an index unit.
- Elevation and slope emerged as significant variables in assessing coastal flood risk [7]. Elevation was measured in meters above sea level (masl), and slope, representing the gradient of the land surface (degree). These data were derived from the CoastalDEM dataset, https://go.climatecentral.org/coastaldem (accessed on 17 September 2021) [41]. The data which were simply resampled from 90 m to a 30 m grid size using bilinear resampling methods to do this given the elevation is continuous variable. As mentioned earlier, in the bilinear interpolation, the values of the four nearest cells are averaged to determine the value of the new cell [50]. Only elevation below 10 m asl and hydrologically connected with coast were included in this screening. In this case, we assumed and treated sub grid features like sand dunes as part of the elevation data, acknowledging the potential limitations of this approach. Subsequently, slope values were generated based on resampled elevation data. Consequently, the slope datasets were in a 30 m grid format.
- Mangrove distribution was incorporated as a key natural barrier. Therefore, we used the geographic feature data of mangrove proximity, as the key variable. This variable was quantified by mangrove distance—the Euclidean distance from each grid to the nearest mangrove point [58–62]. This variable was collected from previous research by Giri et al., (2011), https://data.unep-wcmc.org/datasets/4 (accessed on 8 Juni 2021) [63]. Mangroves are recognized for their ability to attenuate wave energy and reduce water heights, thereby mitigating flood risks [58–62]. These data were represented in an index unit.
- Population data, both baseline and projected, were utilized to assess the relationship between population influence to coastal flood occurrence [5]. The study used the Global Population Projection Grids, acquired from Socioeconomic Data and Applications Center, (SEDAC), https://doi.org/10.7927/q7z9-9r69 (accessed on 15 February

2022). This source provided total population estimates from 2010 to 2100 based on various Shared Socioeconomic Pathways (SSPs) both baseline and SSP 1–5 in 1 km grid size [43]. The data on 2000 were used as the baseline, while data on 2050 and 2100 for five SSPs were used as projection datasets. Population data is in continuous and exhibit gradual changes across geographic areas. Therefore, to harmonize the data into a 30 m grid size, we used bilinear interpolation because it calculates the output value based on the average of the four nearest pixel values, providing a smoother transition and reducing the blocky appearance that can occur with nearest-neighbor interpolation. This is particularly important in population data, where abrupt changes can lead to misinterpretations of demographic distributions [51]. The population data were presented as number of people.

- Settlement types were based on population size and distance to urban centers, called Urban Residential Catchment Areas (URCAs), acquired from Cattaneo et al. (2021) [44]. This study has been adapted and modified into ten categories of urban settlement types to simplify it. URCA types 1 to 7 were retained in this study. URCA types 9–28 were classified into Type 8, rural areas, while the remaining types (URCA type 29 and 30) were maintained and classified as type 9 and type 10, respectively. This classification aids in evaluating the vulnerability of different settlement types to flooding [44]. The data were originally in 90 m grid size in a raster format. We simply resampled into 30 m using nearest-neighbor as the data in a categorical format. These data were presented in an index unit (types).

Following the transformation of all aforementioned data to a 30 m grid size, all variables were subsequently converted and standardized into a grid-based format and consolidated into a feature grid-based table. We stratified the datasets to address the imbalance in coastal flood occurrences, where non-flooding cases were more prevalent. Stratification enhances risk analysis by balancing the dataset, as demonstrated in previous studies [7,64]. We then divided the stratified data into training (70%) and testing (30%) datasets to develop and validate the GeoAI model.

2.2.3. Risk Simulation

This study utilized ensemble machine learning (ML) models—RF, kNN, and ANN—to simulate coastal flood risks. The selection of these models was informed by their proven effectiveness in flood risk assessments and climate change risk assessments, as documented in the literature [65,66]. The RF algorithm, an ensemble learning method, constructs multiple decision trees and aggregates their outputs by majority vote for classification tasks or averaging for regression tasks. RF is known for its high precision and reduced bias, making it ideal for coastal flood risk classification [66]. The kNN algorithm uses the proximity of data points to classify data [67]. In this study, the parameter k was initially set to 5 and tuned to 18 to achieve the highest accuracy. ANNs were employed for pattern recognition and classification tasks [68]. They are particularly effective in capturing complex relationships in data, making them suitable for predicting coastal flood occurrences.

2.3. Evaluation of the Coastal Flood Risk Utilizing the IPCC Risk Approach

A comparison was made using the IPCC risk framework to evaluate the GeoAI model's performance against conventional approaches. The IPCC approach was applied to the entire study area, with key variables standardized and adjusted according to their relevance to hazard, exposure, and vulnerability components [69]. The performance of the IPCC approach was assessed by comparing its risk predictions with historical coastal flood occurrences.

The IPCC approach was applied to the entire study area, with key variables standardized from 0 to 1, where 1 indicates a higher contribution to flood risk. Several adjustments were made:

- ESL: This is used directly as a hazard component, with higher ESL indicating more significant risk.
- Coastline Proximity: Reversed, so areas farther from the coast were assigned lower risk scores.
- Elevation: Reversed, with higher elevations considered less risky.
- Slope: Reversed, with flatter areas assigned higher risk scores due to increased flood susceptibility.
- Mangrove Distance: Reversed, with greater distances from mangroves contributing more to risk.
- Population (SSPs): Treated as a vulnerability component, with higher populations increasing risk.
- Settlement Types: Reversed, assuming rural areas have lower adaptive capacity and higher vulnerability.

Risk scores were calculated using two weighting methods: identical weights for all variables and weights based on Random Forest Feature Importance. This produced a coastal flood risk score from 0 to 1, with 1 indicating a high likelihood of flooding. The IPCC risk results were then compared to historical flood occurrences to evaluate the model's accuracy. This provided a benchmark to assess the GeoAI model's effectiveness. While the IPCC approach offers a standardized method, the GeoAI model may provide more localized and accurate predictions, especially where traditional methods may be less effective.

2.4. Comparison of Model Performance

The model's performance was evaluated using a confusion matrix and classification report. The classification model can make two types of "wrong" predictions. First, the model could predict an area will be flooded when the area is not flooded (false positive). Secondly, the model could predict that an area will not be flooded when the area is flooded (false negative). Avoiding the second point is crucial as it aims to prevent the underestimation of flood damage, which could potentially lead to countries receiving less financial support. Thus, the recall score should be maximized to avoid this issue. The recall is a measure of how many truly relevant results are returned. It was calculated by dividing the number of true positives (TP) by the number of true positives plus the number of false negatives (FN).

A confusion matrix (metrics accuracy) and classification report were used to evaluate the model's performance. The model optimization was performed to tune the model where recall and f1-score are expected to be higher than 60% as a threshold for the model. Only the model that satisfied this score will be used for further estimation and projection. The final coastal flood risk model was then obtained, resulting in a prediction of coastal flood occurrences. Furthermore, this study used these performance tests, namely recall score, precision score, and f1 score, to compare the results of GeoAI models with the IPCC risk approach for coastal flood risk assessments. As explained earlier, the recall score represents the percentage of actual positives that the model correctly identified. The precision score shows the actual negatives that the model correctly identified, and the f1 score is an average of both recall and precision scores.

2.5. Evaluation of Spatial–Temporal Projection of Coastal Flood Occurrence Under Climate Change

The final step involved projecting coastal flood risks spatially and temporally for the years 2050 and 2100. This was achieved by incorporating population projections (using SSPs 1 to 5) and ESLs (based on RCP 4.5 and 8.5 scenarios). The projected variables were applied to training simulation in the selected GeoAI model to generate coastal flood risk maps for these future periods. The coastal flood grids were used to identify and estimate

the populations and settlements at risk. It overlaid the coastal flood occurrence grid with the population and World Settlement Footprint (WSF) map from [70].

In the final step, this section explored the significance of mangroves as Eco-DRR, utilizing the GeoAI approach derived from ML models, mainly the RF. The RF is equipped with an embedded library that identifies the variables that significantly contribute to the target variable or the occurrence of coastal floods. By highlighting the role of mangroves, this paper emphasizes the importance of integrating ecological approaches into disaster risk assessment and further coastal flood management efforts.

2.6. Revealing Mangrove Significance Using Feature Importance Based on RF Model

A feature importance score represents the importance of a particular feature in making predictions. The only RF model that can provide feature significance was available. Thus, regardless of the prediction model employed (with a recall score greater than 60%), the feature significance will only be derived from the RF model in this investigation. Feature significance is determined by calculating the reduction in node impurity, considering the chance of accessing that node. The node probability may be determined by dividing the number of samples that reach the node by the total number of samples. As the value increases, the importance of the trait becomes more significant. This work used the Scikit-learn toolkit to compute the feature's importance in the RF algorithm. RF combines the bagging algorithm with the random subspace method. It uses decision trees as the foundation for the classifier. Scikit-learn found out how important each node in a decision tree was by figuring out the Gini significance, which is the average increase in purity that happens when you split a variable [71]. In this case, feature importance was used to understand each feature's contribution to flood risk prediction.

3. Results

3.1. Coastal Flood Pathways and Key Variables

This study identifies key variables and pathways contributing to coastal flood risk, focusing on geophysical, hydrometeorological, and socioeconomic factors. The selected variables, illustrated in Figure 2, included ESL, coastline proximity, elevation, slope, mangrove distance, population, and settlement types. These variables were subsequently utilized to predict coastal flood occurrence as the target variable. These variables were considered to play a critical role in the occurrence and extent of coastal floods.

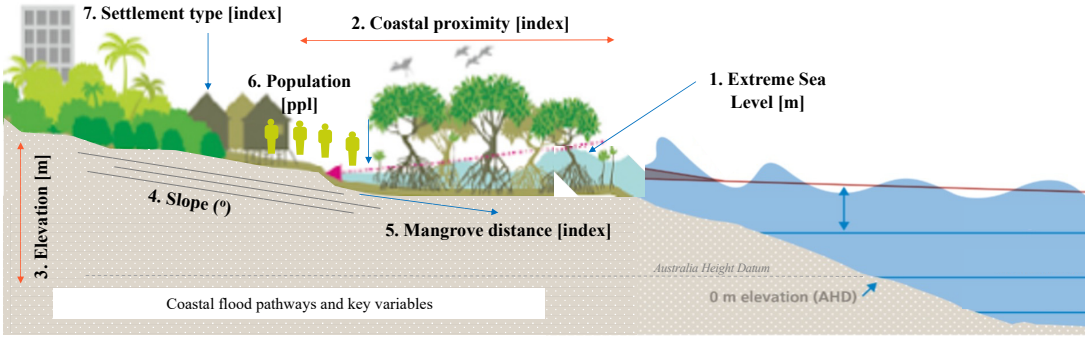

Figure 2. Coastal flood pathways and key variables adapted from [72].

A developed GeoAI approach was demonstrated in El Salvador as a case study to assess the impact of coastal flooding. El Salvador is a Central American nation with a 307 km coastline along the Pacific Ocean. Figure 3 in the study illustrates the coastal flood occurrence in El Salvador between 2000–2018 as the target variable. Upon examination of historical records of coastal floods, a bias (false positive) in the mapping data was identified. This limitation has affected the accuracy of the simulation. Additionally, Figure 3 presented an exploratory data analysis of the critical variables in El Salvador during the

baseline period. The ESLs ranged from 0 to approximately 2 m above sea level. The proximity to the coastline was consistent with the slope and distribution of mangroves. Most areas exhibited a slope of less than 2.5 degrees and were situated within 5000 units of proximity to the coastline. In El Salvador's LECZ, the population density averaged 144 people per grid unit, with a maximum of 812 individuals per grid. The study area in El Salvador encompassed seven towns, eight rural areas, and nine dispersed towns, predominantly comprising rural areas.

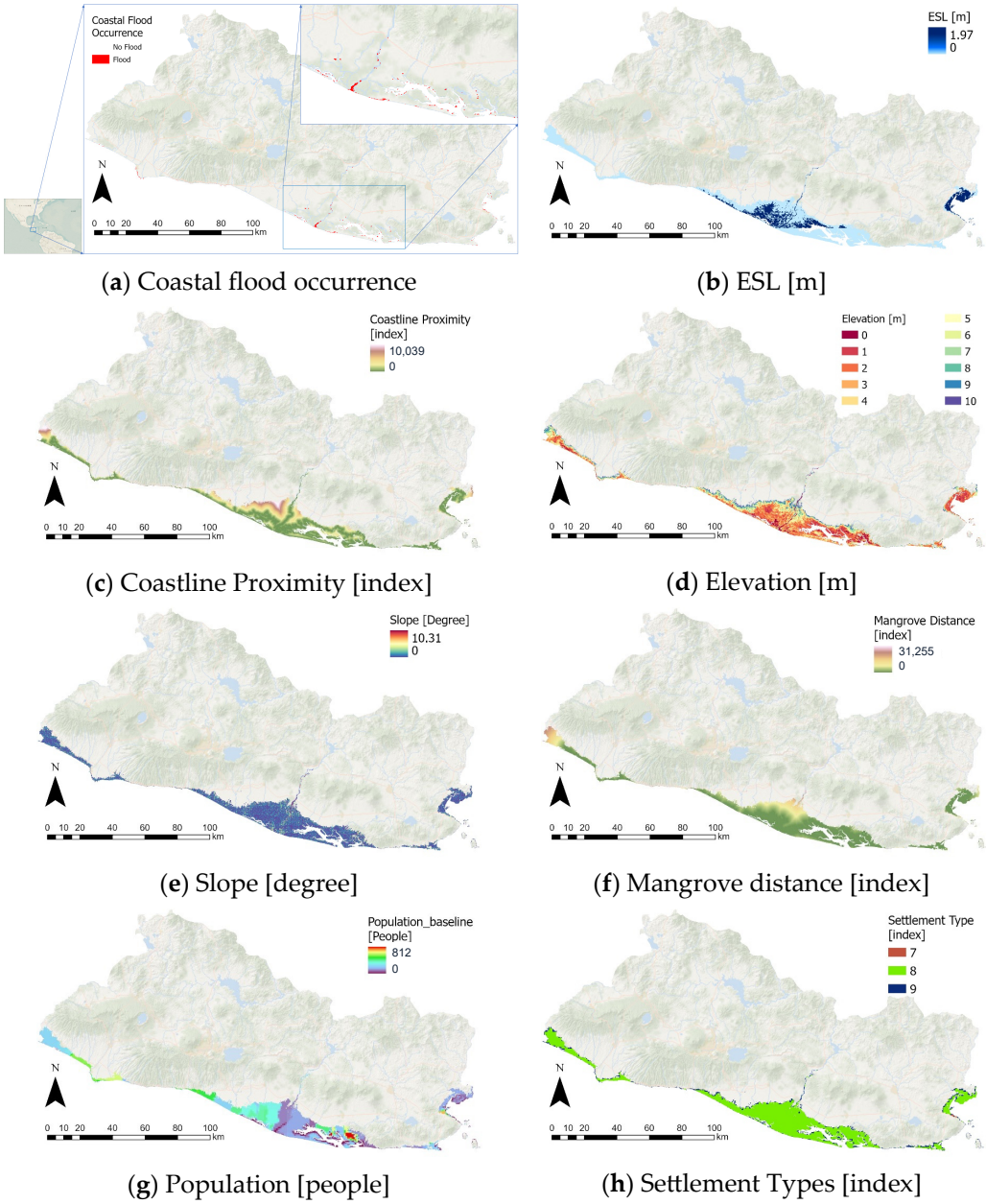

(**a**) Coastal flood occurrence (**b**) ESL [m]

(**c**) Coastline Proximity [index] (**d**) Elevation [m]

(**e**) Slope [degree] (**f**) Mangrove distance [index]

(**g**) Population [people] (**h**) Settlement Types [index]

Figure 3. Coastal flood occurrences and seven key forcing variables in El Salvador.

3.2. Coastal Flood Risk Utilizing the GeoAI Approach

The study utilized three ML models—RF, kNN, and ANN—to assess coastal flood risks in El Salvador following a GeoAI approach. The RF model, an ensemble learning algorithm aggregating multiple decision trees, exhibited robust predictive capability for coastal flood occurrence (Figure 4a). The model's predictions closely matched historical coastal flood maps, demonstrating robustness in spatially identifying areas most susceptible to coastal flooding. In contrast, the kNN model underestimated coastal flood risks,

particularly regarding spatial predictions, as shown in Figure 4c. Meanwhile, the ANN model resulted in poor spatial predictions, as illustrated in Figure 4d. The model identified few coastal flood zones geographically despite being tuned.

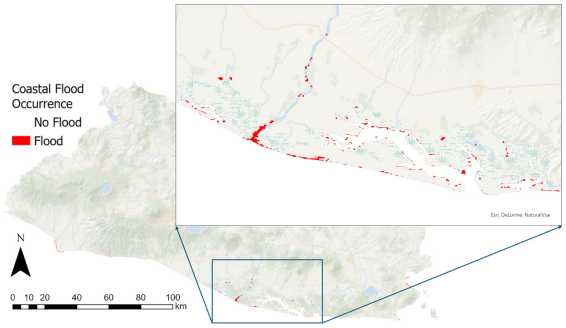

(**a**) Historical Coastal flood occurrence 2000–2018

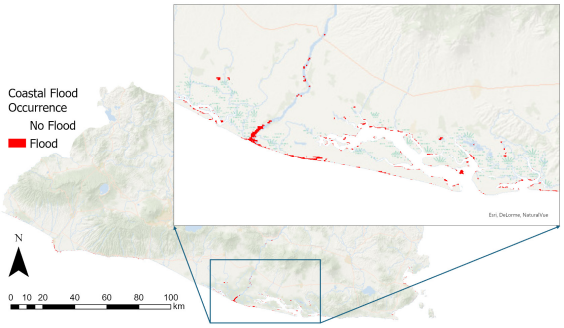

(**b**) Coastal Flood Prediction based on RF Model at the baseline period

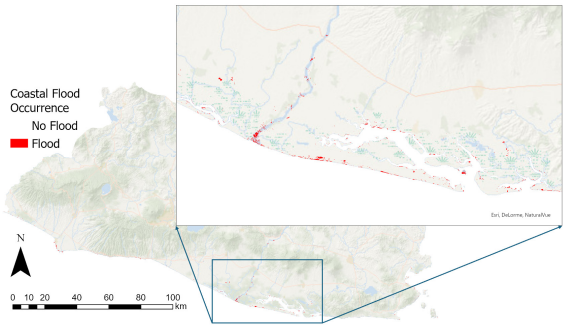

(**c**) Coastal Flood Prediction based on the kNN Model at the baseline period

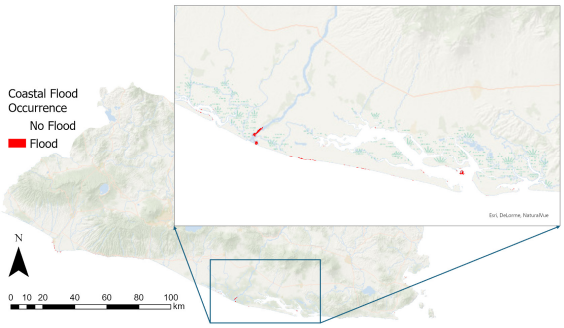

(**d**) Coastal Flood Prediction based on the ANN Model at the baseline period

Figure 4. Comparison of historical coastal flood occurrence 2000–2018 (**a**) and prediction of coastal flood at the baseline period in El Salvador case based on RF model (**b**), kNN model (**c**), and ANN model (**d**).

The confusion matrix and classification report were utilized to evaluate the performance of each ML model, as illustrated in Figure 5. The GeoAI approach, employing the RF model, demonstrated high efficacy in predicting coastal flood occurrence. The RF model attained a precision score of 0.86, a recall of 0.67, and an accuracy of 0.99. However, the model exhibited a substantial false-negative value of 3119. In contrast, the classification report of kNN indicated a precision score of 0.78 and a recall score of 0.39, both inferior to the RF model, with considerable challenges in accurately identifying all instances of coastal flooding. The ANN model's classification report revealed a precision score of 0.79, but its recall was notably low at 0.13 despite an overall accuracy of 0.98.

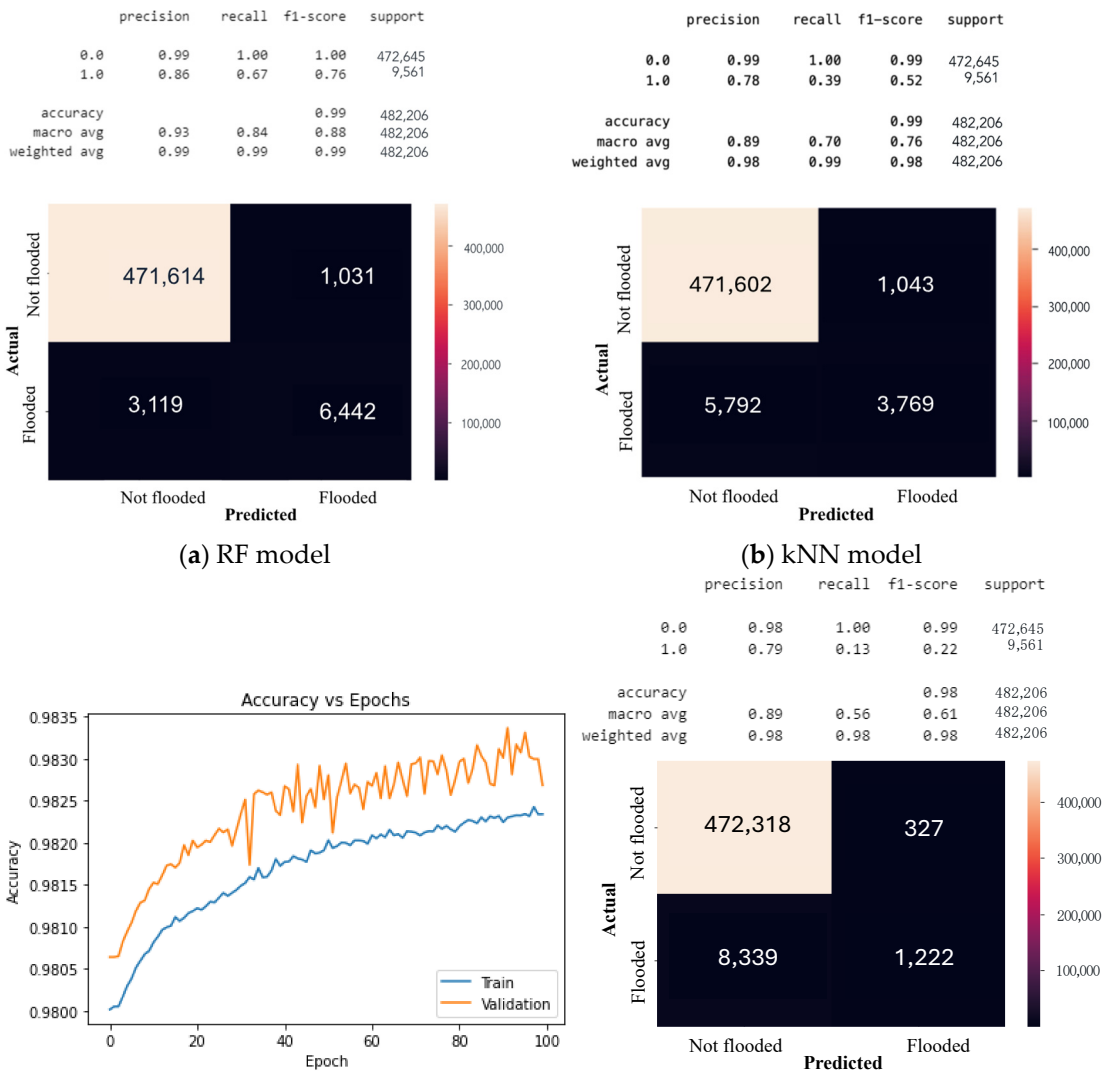

(**a**) RF model (**b**) kNN model

(**c**) ANN model

Figure 5. Comparison of model performance using classification report and accuracy, specifically RF model (**a**), kNN model (**b**), and ANN model (**c**).

3.3. Coastal Flood Risk Utilizing the IPCC Risk Approach

The IPCC has developed a risk approach to assess coastal flood risk based on the combination of exposure, vulnerability, and hazard [73]. In this study, the IPCC risk approach was applied to assess the coastal flood risk in El Salvador using two methods: the same weights for all variables and adjusted weights based on RF feature importance results (Figure 6). RF is the only model that provides feature importance scores, which is the primary reason for its utilization in this study. These feature importance scores represent a metric that indicates the significance of a particular variable in making predictions. They demonstrate the relative importance of each variable in contributing to coastal flood risk. Figure 6 illustrates the feature importance score of each variable, considering future changes (utilizing updated datasets on population and ESL). A higher score indicates greater importance of the variable. The feature importance scores indicated that the mangrove proximity variable exhibited the highest contribution, followed by population, coastline distribution, and settlement types, respectively. These scores were utilized for the weighting in the IPCC risk approach.

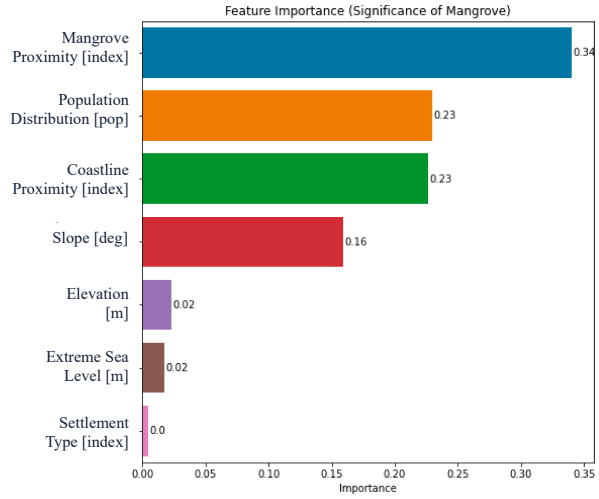

Figure 6. Feature importance.

The results were presented on a map that showed the coastal flood risk range from 0 to 1, where 1 indicates a more severe risk. The map was overlaid with historical coastal flood data indicated in red (Figure 7—top panel). Both weighting methods were able to detect coastal flood risk in a spatial manner. However, evaluating the same weighting method between coastal flood risk and historical occurrence revealed a higher incidence of coastal floods in the 0.5 risk score (Figure 7—bottom panel)., suggesting that the risk approach did not yield satisfactory results. Meanwhile, on the adjusted weight, a risk score over 0.7 detected more coastal flood occurrences, which indicated that the IPCC risk approach with this weighting method could detect the coastal flood.

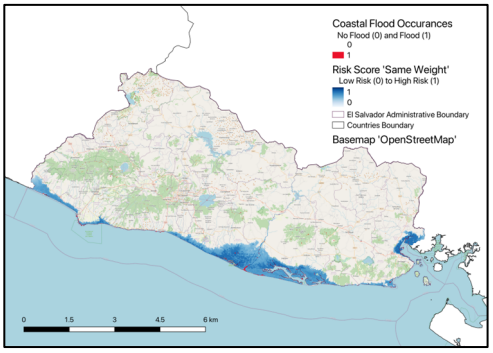

(**a**) IPCC risk approach–the same weight method

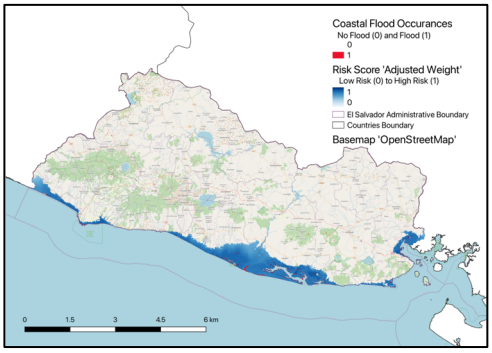

(**b**) IPCC risk approach–adjusted weight method

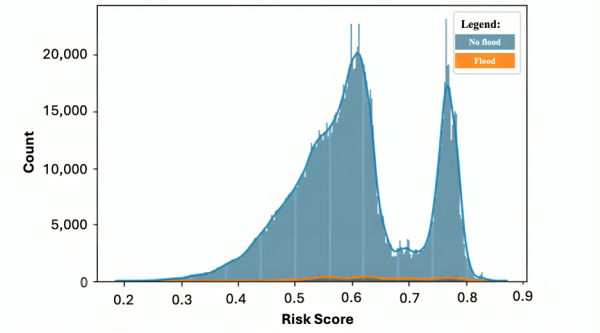

(**c**) Performance of the IPCC risk approach with same weight method

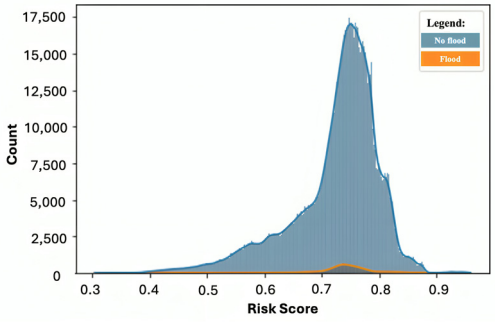

(**d**) Performance of the IPCC risk approach with adjusted weight method

Figure 7. Coastal flood risk assessment and its performance based on the IPCC risk approach overlaid with historical flood data in El Salvador. The same weighting method (**a**) and its performance (**c**) and the adjusted weight method based on RF feature importance (**b**) and its performance (**d**).

3.4. Comparison Between the GeoAI Model and the IPCC Risk Approach

This study compared the performance of GeoAI models with the IPCC risk approach for coastal flood risk assessment based on the model results (recall score, precision score, and f1-score), as detailed in Table 2. The RF model was chosen for its superior performance, demonstrating higher precision, recall, and accuracy than the kNN and ANN models. Specifically, the RF model achieved a precision score of 0.86, correctly identifying 86% of the predicted positive coastal flood cases. The recall score was 0.67, indicating the model's ability to correctly identify 67% of the actual positive coastal flood cases. Furthermore, the RF model exhibited an impressive accuracy score of 0.99, accurately classifying 99% of the coastal flood cases.

In contrast, the IPCC risk approach was evaluated using two different methods: equal weighting for all variables and adjusted weighting based on RF feature importance. The results showed that the same weighting method was less effective, with an f1 score of 0.49, showed the lowest accuracy in terms of detecting coastal flood risk. On the other hand, the adjusted weighting method improved the detection of coastal flood occurrences spatially, suggesting that the IPCC risk approach with this method could better identify flood risks. Yet, all scores showed poor results with only 0.01 score.

Table 2. Evaluation performance of the GeoAI and IPCC risk approach.

Metric Accuracy	RF	kNN	ANN	IPCC Risk Same Weight	IPCC Risk Adjusted Weight
TN	471,614	471,602	472,318	74,396	465,421
FP	1031	1043	327	398,248	9481
FN	3119	5792	8339	404	7224
TP	6442	3769	1222	9158	80
Total Observation Data	482,206	482,206	482,206	482,206	482,206
Recall Score	0.67	0.39	0.13	0.96	0.01
Precision Score	0.86	0.78	0.79	0.02	0.01
f1-score	0.77	0.59	0.46	0.49	0.01

3.5. Spatial–Temporal Projection of Coastal Flood Occurrence Under Climate Change

This study employed the RF model, identified as the best model, to project the occurrence of coastal floods under future climate change scenarios. The RF model demonstrated high accuracy when applied to future datasets (Figure 8); however, there was a noted decline in recall, indicating that the model may overlook some areas at risk of coastal flooding. This issue underscores the necessity of fine-tuning model parameters or incorporating additional data to enhance recall and overall predictive performance. Specifically, four projection datasets were selected based on their high recall scores to predict coastal flood occurrences in 2050 and 2100. For period 2050, it included RCP4.5 with SSP3 (cf_rf_45_SSP3) and RCP8.5 with SSP4 (cf_rf_85_SSP4). While for period 2100, it included RCP4.5 with SSP3 (cf_rf_45_SSP3) and RCP8.5 with SSP2 (cf_rf_85_SSP2).

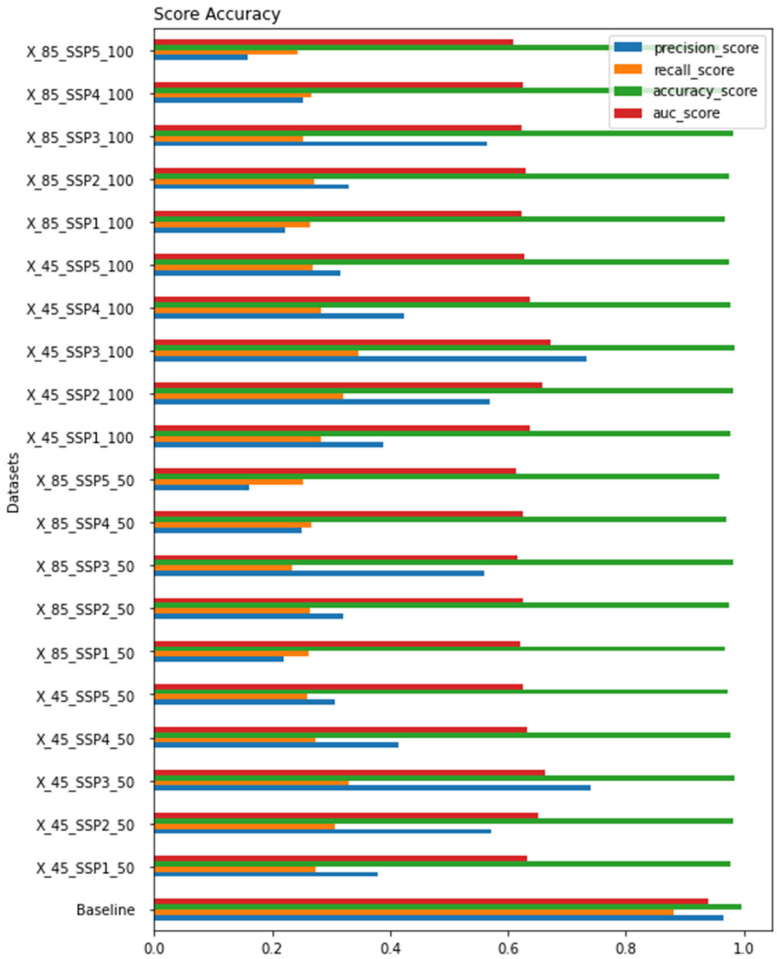

Figure 8. RF model evaluation report for baseline and projection.

The geographical analysis for El Salvador, based on the aforementioned four projection datasets, indicated a projected rise in coastal flood spots, particularly under future climatic scenarios, as seen in Figure 9. The total number of predicted coastal flood points in the coastal zone was 29,101, which was slightly lower by 2769 points compared to historical occurrences. For instance, in the RCP4.5 scenario with SSP1 in 2050, the predicted number of coastal floods was 22,958, lower than both the baseline model and historical data. However, in 2100, this number increased to 38,268, indicating a long-term impact of climate change. Under the RCP8.5 scenario with SSP1 in 2050, the predicted number of floods was 23,297, which also increased to 37,923 by 2100. Temporal comparisons within the RCP4.5 scenario indicated a gradual decrease in coastal flood occurrences from 22,958 points in 2050 (SSP1_50) to 13,321 points in 2100 (SSP3_100). Conversely, under the RCP8.5 scenario, flood occurrences increased in certain cases, particularly in SSP5, where the number of predicted flood points rose from 27,099 in 2050 to 49,092 in 2100. This trend underscores the significant impact of both climate and socioeconomic factors on future coastal flood risks.

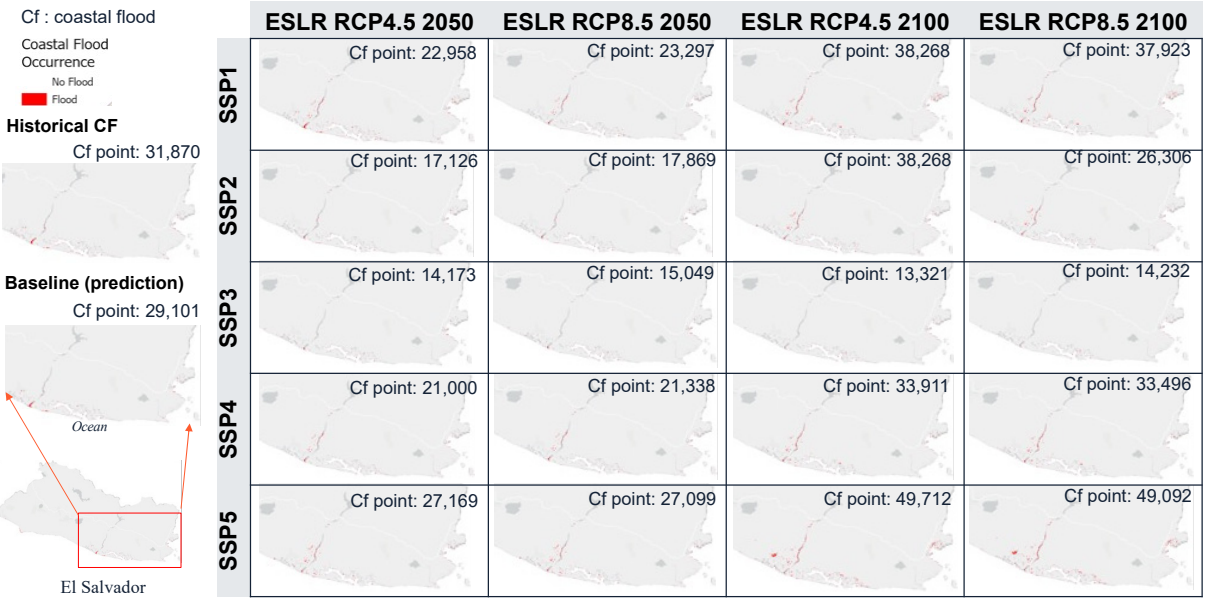

Figure 9. Coastal flood prediction in the baseline and projection periods in 2050 and 2100 using RCP4.5 and RCP8.5, as well as SSP1 to SSP5 scenarios based on RF Model results in El Salvador. Cf is defined as the frequency of coastal flood occurrence.

To identify future coastal flood occurrence, this study also used all the projection datasets (Figure 10). This combination spanned RCP4.5 and 8.5 in the period 2050 and 2100 considering SSP1 to SSP5. In total, there were 20 scenarios compare to baseline projection and historical coastal flood occurrence. The projections indicated an increase in coastal flood occurrences over time, with the extent of the increase depending on the selected scenario, as illustrated in Figure 10. Notably, the highest projected percentage of coastal flood occurrence was found in the "cf_rf_45_SSP5_100" scenario, predicting that 3.09% of coastal floods would occur by 2100, an increase of 1.28% from the baseline. In contrast, the lowest projected percentage was observed in the "cf_rf_45_SSP3_100" scenario, with a value of 0.83%. When comparing the periods, coastal flood occurrence was generally higher in 2100 than in 2050, illustrating the influence of climate and socioeconomic changes on increasing flood risks over time. The projections also showed that the highest coastal flood percentages were associated with SSP5 scenarios in both RCP4.5 and RCP8.5, while the lowest percentages were linked to SSP3 scenarios.

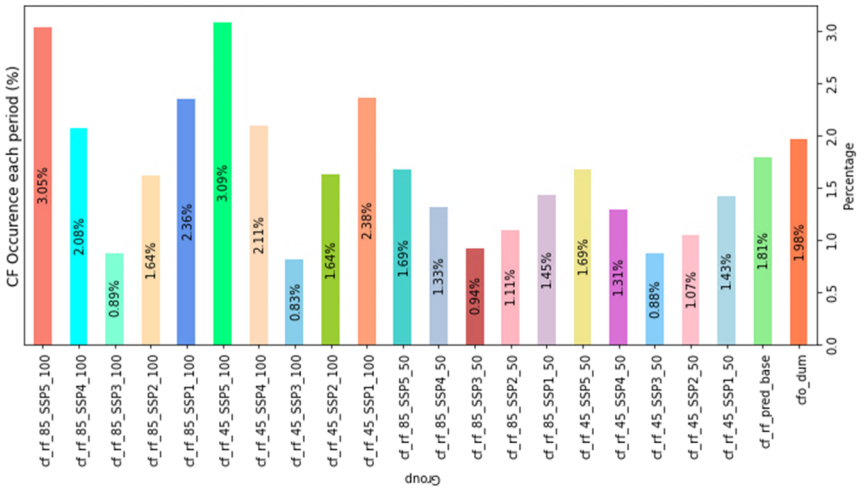

Figure 10. Percentage of coastal flood occurrence at baseline and projection based on RF Model. Cf means coastal flood, while cfo represents coastal flood occurrence.

3.6. Mangrove Significance as Eco-DRR on Coastal Flood Risk Reduction

The study utilized the GeoAI approach to assess the impact of various variables on coastal flood occurrences, with particular emphasis on the role of mangroves. The RF model revealed that proximity to mangroves was the most significant variable influencing coastal flood risk, achieving a feature importance score of 0.34. The results demonstrated a negative relationship between mangrove proximity and flood occurrence, suggesting that the closer an area is to mangroves, the higher the likelihood of flood occurrence. Specifically, coastal floods were more frequent within 0–500 m of continuous mangroves, with over 11,000 flood points observed in this range, as illustrated in Figure 11. In contrast, regions further than 1500 m from mangroves, particularly areas without continuous mangrove coverage, experienced significantly fewer floods. Spatial analysis of the El Salvador coastline further supported these findings, showing that areas with dense mangrove presence had substantially fewer flood points than regions lacking continuous mangrove cover. In areas with continuous mangroves, only 3786 grids of coastal floods were recorded, while 371,751 grids in the same region were flood-free. Additional variables, such as coastline proximity and population density, also played a role in flood risk, each with an importance score of 0.23.

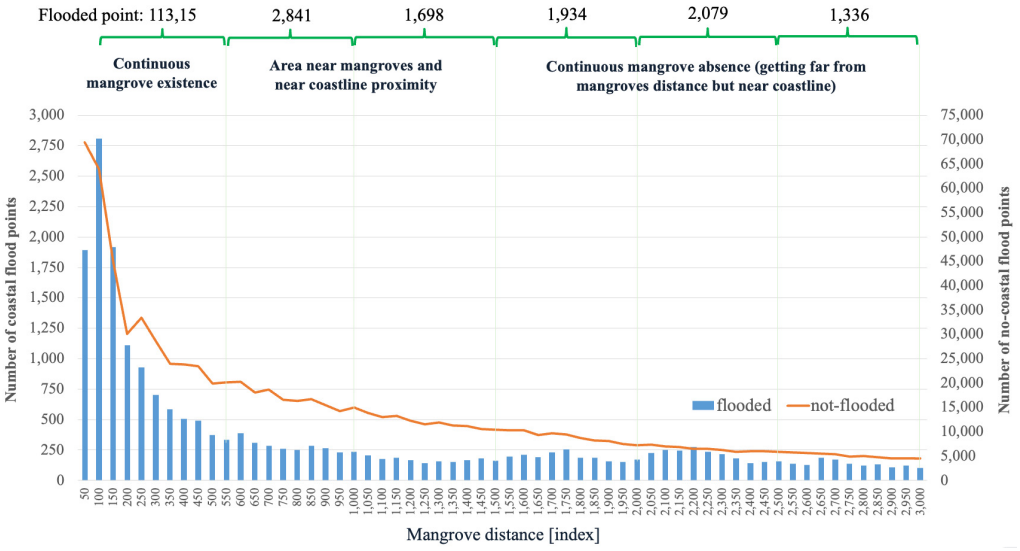

Figure 11. Coastal flood prediction in the baseline and projection periods in 2050 and 2100 using RCP4.5 and RCP8.5, as well as SSP1 to SSP5 scenarios based on RF Model results in El Salvador.

4. Discussion

Identifying coastal flood pathways and key variables is essential for effective flood risk management. Using coastal flood occurrence as a binary variable in the GeoAI model provided a clear framework for simulating flood risks. However, potential biases in the flood occurrence data, such as false positives, must be carefully considered to ensure the accuracy of the results [40]. The seven key variables identified have revealed their relationship to coastal flood occurrences. Including ESL as a key variable reflects the growing urgency of addressing sea-level rise. The study's findings underscore the need for incorporating TWL in flood risk assessments. The probabilistic projections of ESL under different emission scenarios offer a robust foundation for long-term flood risk management strategies [74,75]. Furthermore, the study reaffirmed the significance of elevation and slope in determining coastal flood risks. Low-lying areas with low gradient slopes are particularly vulnerable to flooding, emphasizing the importance of detailed topographic data in flood risk assessments. According to previous studies, slope contributed to over 25% of flood risk prediction [76].

In integrating geographic features, coastal proximity and mangrove distance were also found essential for the simulation. Mangroves are crucial in mitigating flood risks, acting as natural barriers that reduce wave energy and water heights. The inclusion of mangrove distance as a variable in the model highlights the importance of preserving these ecosystems for coastal flood protection. The study's findings align with previous research that has demonstrated the effectiveness of mangroves in reducing the impact of coastal floods [58–62]. The study's focus on population distribution and settlement types adds a critical dimension to coastal flood risk prediction. By considering SSP data on projected population growth, the research provides valuable insights into the future impacts of flooding on different settlement types. The classification of settlements based on their proximity to urban centers and population density helps prioritize areas for adaptation efforts, particularly those most at risk [4,5,44].

The GeoAI-based coastal flood risk assessment in El Salvador revealed that the RF model outperformed the kNN and ANN models' prediction accuracy and spatial distribution of coastal flood risks. The RF model's high precision and accuracy indicate its robustness in predicting coastal flood events and its potential value in disaster preparedness and response strategies [77]. However, the model's significant number of false negatives raises concerns, as these missed predictions could have critical implications for disaster risk management, particularly in areas where the model does not sufficiently capture coastal flood risks. This limitation suggests that additional variables, such as land-use changes and wave dynamics, might need to be incorporated into the model to enhance its predictive capability [78].

The kNN model, while simpler and easier to implement, demonstrated significant limitations in predictive accuracy, particularly in spatial predictions. The lower precision and recall scores compared to the RF model suggest that the kNN model may not fully capture the complexity of coastal flood dynamics. The underestimation of flood risks and the higher number of false positives could lead to unnecessary emergency responses, highlighting the importance of model selection in risk assessment studies. The results align with previous studies that found kNN models to be less effective than RF in similar contexts [7,78].

Conversely, the ANN model, while theoretically capable of capturing complex patterns in data, underperformed in this study. Even after optimization, the model predicted a minimal number of coastal flood occurrences. The ANN model's poor performance, particularly its low recall score, points to potential issues related to class imbalance in the training data. The model's tendency to predict the majority class (non-flooding events) more frequently than the minority class (flooding events) likely contributed to its inability to accurately predict coastal floods [68]. This finding underscores the importance of addressing data imbalances when applying ANN models in environmental risk assessments. Additionally, the model's limited consideration of relevant variables, such as typhoon frequency and topographic wetness index, may have further hindered its predictive capability [64,65,77].

The comparison between the GeoAI Model and IPCC risk results underscores the effectiveness of the GeoAI approach, particularly the RF model, in predicting coastal flood risks. The superior performance of the RF model aligns with previous studies that demonstrated its high sensitivity and effectiveness in flood hazard risk assessments. Wang et al. (2015) highlighted the RF model's ability to efficiently handle large databases and provide accurate predictions by estimating the importance of specific variables [79]. Similarly, its use in modeling urban coastal flood severity from crowd-sourced data further validated its low false negative rate and robust predictive capabilities [66]. In contrast, the IPCC risk approach, which relies heavily on historical data and a weighting method, was found to be less effective in capturing the complex dynamics of coastal flood occurrences. The IPCC risk approach requires human intervention (assigning weights to features) and has limitations in handling multi-dimensional data [80]. The equal weighting method, in particular, failed to provide reliable risk assessments, as evidenced by the concentration of flood

occurrences at a mid-range risk score. However, when the IPCC approach was adjusted based on RF feature importance, its performance improved, indicating that variable weighting plays a crucial role in risk detection accuracy. The results of this study are consistent with previous studies that also found the limitations of the IPCC risk approach in predicting coastal flood risk accurately. For instance, Lin (2019) [81] noted that the IPCC risk approach underestimated the flood risk in some regions due to the lack of consideration of local topography and land cover characteristics. In summary, utilizing the GeoAI approach advances the accuracy of the coastal flood risk assessment.

The advantages of the GeoAI approach, specifically its ability to integrate diverse data sources, including spatial and temporal data, were evident in its superior performance over the IPCC approach. GeoAI's capability to analyze complex datasets and identify patterns that traditional methods might overlook was crucial in enhancing coastal flood risk predictions. This aligns with findings from Li and Hsu (2022), who demonstrated the efficacy of GeoAI and deep learning in accurately assessing coastal flood risk in specific areas [21]. The comparison between the GeoAI and IPCC approaches also highlights the flexibility and tunability of ML models like RF, which can be optimized to achieve high accuracy, unlike the more rigid IPCC approach. Additionally, GeoAI was not influenced by the weighting method that challenged the IPCC risk approach. This study, therefore, reinforces the potential of GeoAI as a powerful tool for coastal flood risk assessment, offering more detailed and reliable insights for risk management and disaster preparedness. The findings contribute to the growing body of literature advocating for the integration of advanced GeoAI methodologies in environmental risk assessments, particularly in the context of climate-induced coastal flooding [19–21,82].

The spatial-temporal analysis underscores the effectiveness of the RF model in projecting future coastal flood occurrences under various climate and socioeconomic change scenarios. Despite its effectiveness, there was a slight decline in recall, suggesting that the model could underestimate risks in some areas. Based on RF projections of coastal flood occurrences, the findings are consistent with existing literature, which indicates a rising trend in coastal flood risk due to factors such as sea-level rise and increased storm surges [74,83,84]. The variations in coastal flood occurrences across different SSPs and RCPs highlight the significant role of climate and socioeconomic factors in influencing flood risks. Specifically, the higher flood percentages associated with SSP5 scenarios suggest that regions with fossil-fuel-driven development may be more vulnerable to coastal flooding, aligning with the assumptions of the RCP8.5 scenario regarding higher greenhouse gas emissions and more severe climate impacts [85]. The spatial analysis of coastal flood occurrences in El Salvador further illustrates the model's utility in identifying regions at heightened risk. The increased predicted flood points over time, particularly under RCP8.5, indicate the potential for more severe flooding, necessitating proactive measures to mitigate these risks. The comparison between different periods within the RCP4.5 and RCP8.5 scenarios underscores the complex interplay between climate change and socioeconomic developments in shaping future flood risks.

To reveal the contribution of mangroves in reducing coastal flood risk, the feature importance results strongly emphasize the importance of mangroves as critical natural barriers against coastal floods, aligning with previous studies highlighting their role in mitigating flood risks [59]. The study revealed that proximity to mangroves significantly reduces flood occurrences, as observed in the El Salvador region. Mangrove proximity contributed one-third of the flood risk prediction (0.34), while coastline proximity accounted for nearly one-quarter (0.23), as shown in Figure 6. This finding is consistent with research demonstrating that mangrove belts—whether thousands or hundreds of meters wide—can significantly decrease the impact of coastal flooding by reducing storm surge height, wave energy, and wind velocity [8,58,61,62].

Mangroves' protective capacity stems from their complex root systems, which stabilize coastlines, reduce erosion, and attenuate wave forces. Their ability to reduce storm surge heights by up to 66%, as observed in regions like the Philippines and Vietnam,

underscores their effectiveness in protecting vulnerable coastal zones [58,60]. In El Salvador, areas with continuous mangrove cover experienced fewer floods, reinforcing the hypothesis that intact mangrove ecosystems play a crucial role in flood mitigation.

While other variables, such as coastline proximity and population density, were also crucial in predicting flood risk, their influence was secondary to that of mangroves. The results highlight the need to prioritize the preservation and restoring mangrove ecosystems as a nature-based solution for coastal flood risk reduction. This finding is consistent with global research underscoring mangroves' role in reducing flood heights, duration, and impacts in low-lying coastal areas [14,59–61].

Furthermore, we emphasized the low contribution of ESL (2%) in the coastal flood risk prediction. Previous studies have revealed that ESL was one of the key factors influencing the coastal flood hazard between 2000 and 2100 [86,87], although the percentage contribution was not mentioned. In this study, we used the point data of ESL, which acknowledges the combination of the mean sea level, tides, waves, and storm surges [39]. However, our limitation was shown in spatialization into grid-based data format, resulting in higher bias, which affects the ESL contribution results in the model.

Additionally, ESL's low importance score was also attributed to the local characteristics of the interaction of ESL with other variables, such as the sole factor of tide and wave, as well as geomorphology [33,34,88], which the study has omitted. The absence of wave-specific data in the current model limits the direct assessment of wave overtopping and inundation as contributing factors. The waves were recognized as one of the main physical drivers of wave overtopping and inundation in El Salvador [46]. For instance, the case of sea swell events from April to May 2015 led to extreme coastal flooding in El Salvador, with 268 m of inundation and extreme erosion of 268 m [46]. As mentioned earlier, the inter-play between waves and tides could influence nearshore wave heights, increasing the danger of flooding at elevated water levels [33,34]. Moreover, previous studies have found that mean tide was the second highest contributor to compound flood in coastal zones in addition to rainfall [7]. Therefore, further research should explore the concept of calculating the contribution of wave dynamics, tide and surge heights [7,74], to provide a more comprehensive analysis of physical drivers influencing coastal flooding.

5. Conclusions

This study provides critical insights into the role of GeoAI models, particularly RF, in predicting coastal flood risks in El Salvador, revealing their advantages over traditional methods like the IPCC approach. The research successfully identified key coastal flood pathways and areas of heightened vulnerability by integrating key variables such as ESL, elevation, slope, coastal proximity, mangrove ecosystems, population, and settlement types to predict coastal flood occurrences. The incorporation of mangrove proximity into the model highlighted the significant protective role of mangroves as natural barriers, consistent with existing research that underscores their effectiveness in reducing flood risks. Additionally, the study demonstrates that low-lying, low-gradient areas with limited natural defenses are particularly susceptible to flooding, underscoring the importance of detailed topographic and geographic data in flood risk assessments. The model's inclusion of socioeconomic variables, such as population density and settlement type, offers a more nuanced understanding of flood exposure and potential future impacts under various climate change scenarios. In particular, the research emphasizes the importance of considering future urbanization trends and population growth in flood risk management strategies.

Comparison results showed that the RF model outperformed the kNN and ANN models in predicting coastal flood risk accuracy and spatial distribution. However, its tendency to produce false negatives underscores the need for further refinement, possibly by including additional variables such as land-use changes and climate variability. Despite these limitations, the RF model's ability to integrate diverse data sources and its flexibility in handling complex datasets make it a valuable tool for coastal flood risk assessments.

Moreover, the spatial-temporal projections indicate that future flood risks are likely to increase due to sea-level rise and more frequent extreme weather events, particularly under high-emission scenarios such as RCP8.5. This finding highlights the urgency of implementing proactive adaptation measures, especially in regions projected to face higher flood percentages under fossil fuel-driven development scenarios.

This study's findings strongly advocate for the preservation and restoring mangrove ecosystems as a critical nature-based solution for eco-DRR. Future research should aim to improve model accuracy by incorporating dynamic factors such as land-use changes and refining the approach to address false negatives. Additionally, integrating climate and socioeconomic scenarios into flood risk assessments will be essential for developing adaptive strategies that protect vulnerable coastal populations and infrastructure in the face of accelerating climate change.

Supplementary Materials: The following supporting information can be downloaded at: www.mdpi.com/xxx/s1, Table S1: Selection and justification of key variables.

Author Contributions: T.A.: Data Curation, Investigation, Methodology, Analysis, Writing—Original draft preparation; M.D.S.: Review and Edit, supervision and Research administration; K.K.: Supervision, Review & Edit, Conceptualization; K.F.: Conceptualization, Resources. All authors have read and agreed to the published version of the manuscript.

Funding: This research was supported by JST SPRING, Grant Number JPMJSP2108 and funded by Asia Pacific Network for Global Change Research, Grant Number CRRP2022-06MY-Muslim project.

Data Availability Statement: Data will be made available on request. We developed a custom Python script for data preprocessing and analysis. The code is available upon request from the corresponding author. Spatial data were prepared using ArcGIS Pro software (version 2.8, University of Tokyo).

Acknowledgments: This study was supported by the Urban Sustainability Science Lab, Department of Urban Engineering, The University of Tokyo, and the Support for Pioneering Research Initiated by Next Generation (SPRING) of the Japan Science and Technology Agency (JST) grant. Moreover, it was partly supported by the Asia Pacific Network for Global Change Research under the CRRP2022-06MY-Muslim project.

Conflicts of Interest: The authors declare no conflicts of interest.

References

1. IPCC Summary for Policymakers. *Global Warming of 1.5 °C. An IPCC Special Report on the Impacts of Global Warming of 1.5 °C Above Pre-Industrial Levels and Related Global Greenhouse Gas Emission Pathways, in the Context of Strengthening the Global Response To*; IPCC AR-5; Masson-Delmotte, V.P., Zhai, H.-O., Pörtner, D., Roberts, J., Skea, P.R., Shukla, A., Pirani, W., Moufouma-Okia, C., Péan, R., Pidcock, S., et al., Eds.; World Meteorological Organization: Geneva, Switzerland, 2018; 32p.
2. Lorie, M.; Neumann, J.E.; Sarofim, M.C.; Jones, R.; Horton, R.M.; Kopp, R.E.; Fant, C.; Wobus, C.; Martinich, J.; O'Grady, M.; et al. Modeling Coastal Flood Risk and Adaptation Response under Future Climate Conditions. *Clim. Risk Manag.* **2020**, *29*, 100233. https://doi.org/10.1016/j.crm.2020.100233.
3. *IPCC, 2021: Climate Change 2021: The Physical Science Basis. Contribution of Working Group I to the Sixth Assessment Report of the Intergovernmental Panel on Climate Change;* Masson-Delmotte, V., P. Zhai, A. Pirani, S.L. Connors, C. Péan, S. Berger, N. Caud, Y. Chen, L. Goldfarb, M.I. Gomis, M. Huang, K. Leitzell, E. Lonnoy, J.B.R. Matthews, T.K. Maycock, T. Waterfield, O. Yelekçi, R. Yu, and B. Zhou (eds.). Cambridge University Press, Cambridge, United Kingdom and New York, USA, 2021; ISBN 978-1-00-915789-6.
4. McGranahan, G.; Balk, D.; Anderson, B. The Rising Tide: Assessing the Risks of Climate Change and Human Settlements in Low Elevation Coastal Zones. *Environ. Urban.* **2007**, *19*, 17–37. https://doi.org/10.1177/0956247807076960.
5. Hauer, M.E.; Hardy, D.; Kulp, S.A.; Mueller, V.; Wrathall, D.J.; Clark, P.U. Assessing Population Exposure to Coastal Flooding Due to Sea Level Rise. *Nat. Commun.* **2021**, *12*, 6900. https://doi.org/10.1038/s41467-021-27260-1.
6. Hinkel, J.; Lincke, D.; Vafeidis, A.T.; Perrette, M.; Nicholls, R.J.; Tol, R.S.; Marzeion, B.; Fettweis, X.; Ionescu, C.; Levermann, A. Coastal Flood Damage and Adaptation Costs Under 21st Century Sea-Level Rise. *Proc. Natl. Acad. Sci. USA* **2014**, 111, 3292–3297. https://doi.org/10.1073/pnas.1222469111.
7. Park, S.-J.; Lee, D.-K. Prediction of Coastal Flooding Risk under Climate Change Impacts in South Korea Using Machine Learning Algorithms. *Environ. Res. Lett.* **2020**, *15*, 94052. https://doi.org/10.1088/1748-9326/aba5b3.

8. Reguero, B.G.; Beck, M.W.; Bresch, D.N.; Calil, J.; Meliane, I. Comparing the Cost Effectiveness of Nature-Based and Coastal Adaptation: A Case Study from the Gulf Coast of the United States. *PLoS ONE* **2018**, *13*, e0192132.
9. Anderson, D.L.; Ruggiero, P.; Mendez, F.J.; Barnard, P.L.; Erikson, L.H.; O'Neill, A.C.; Merrifield, M.; Rueda, A.; Cagigal, L.; Marra, J. Projecting Climate Dependent Coastal Flood Risk with a Hybrid Statistical Dynamical Model. *Earth's Future* **2021**, *9*, e2021EF002285. https://doi.org/10.1029/2021EF002285.
10. Atmaja, T.; Fukushi, K. Empowering geo-based ai algorithm to aid coastal flood risk analysis: a review and framework development. *ISPRS Ann. Photogramm. Remote Sens. Spat. Inf. Sci.* **2022**, *V-3–2022*, 517–523. https://doi.org/10.5194/isprs-annals-V-3-2022-517-2022.
11. Hasan Tanim, A.; Goharian, E. Developing a Hybrid Modeling and Multivariate Analysis Framework for Storm Surge and Runoff Interactions in Urban Coastal Flooding. *J. Hydrol.* **2021**, *595*, 125670. https://doi.org/10.1016/j.jhydrol.2020.125670.
12. Couasnon, A.; Sebastian, A.; Morales-Nápoles, O. A Copula-Based Bayesian Network for Modeling Compound Flood Hazard from Riverine and Coastal Interactions at the Catchment Scale: An Application to the Houston Ship Channel, Texas. *Water* **2018**, *10*, 1190.
13. Sheng, Y.P.; Paramygin, V.A.; Rivera-Nieves, A.A.; Zou, R.; Fernald, S.; Hall, T.; Jacob, K. Coastal Marshes Provide Valuable Protection for Coastal Communities from Storm-Induced Wave, Flood, and Structural Loss in a Changing Climate. *Sci. Rep.* **2022**, *12*, 3051. https://doi.org/10.1038/s41598-022-06850-z.
14. Fernández-Díaz, V.Z.; Turriza, R.A.C.; Castilla, A.K.; Hinojosa-Huerta, O. Loss of Coastal Ecosystem Services in Mexico: An Approach to Economic Valuation in the Face of Sea Level Rise. *Front. Mar. Sci.* **2022**, *9*, 1077. https://doi.org/10.3389/fmars.2022.898904.
15. Haiyun, W.; Searle, G.; Wang, S.; Liu, Y. Understanding Residential Relocation Choices in Coastal Cities in the Face of Climate Change. *Findings* **2021**. https://doi.org/10.32866/001c.23722.
16. Takagi, H. "Adapted Mangrove on Hybrid Platform"—Coupling of Ecological and Engineering Principles against Coastal Hazards. *Results Eng.* **2019**, *4*, 100067. https://doi.org/10.1016/j.rineng.2019.100067.
17. He, Q.; Silliman, B.R. Climate Change, Human Impacts, and Coastal Ecosystems in the Anthropocene. *Curr. Biol.* **2019**, *29*, R1021–R1035. https://doi.org/10.1016/j.cub.2019.08.042.
18. Lai, Y.; Li, J.; Chen, Y.D.; Chan, F.K.S.; Gu, X.; Huang, S. Compound Floods in Hong Kong: Hazards, Triggers, and Socio-Economic Consequences. *J. Hydrol. Reg. Stud.* **2023**, *46*, 101321. https://doi.org/10.1016/j.ejrh.2023.101321.
19. Gonzales-Inca, C.; Calle, M.; Croghan, D.; Torabi Haghighi, A.; Marttila, H.; Silander, J.; Alho, P. Geospatial Artificial Intelligence (GeoAI) in the Integrated Hydrological and Fluvial Systems Modeling: Review of Current Applications and Trends. *Water* **2022**, *14*, 2211. https://doi.org/10.3390/w14142211.
20. Janowicz, K.; Gao, S.; McKenzie, G.; Hu, Y.; Bhaduri, B. GeoAI: Spatially Explicit Artificial Intelligence Techniques for Geographic Knowledge Discovery and Beyond. *Int. J. Geogr. Inf. Sci.* **2020**, *34*, 625–636. https://doi.org/10.1080/13658816.2019.1684500.
21. Li, W.; Hsu, C.-Y. GeoAI for Large-Scale Image Analysis and Machine Vision: Recent Progress of Artificial Intelligence in Geography. *ISPRS Int. J. Geo-Inf.* **2022**, *11*, 385. https://doi.org/10.3390/ijgi11070385.
22. Mosavi, A.; Ozturk, P.; Chau, K. Flood Prediction Using Machine Learning Models: Literature Review. *Water* **2018**, *10*, 1536. https://doi.org/10.3390/w10111536.
23. Chang, F.-J.; Hsu, K.; Chang, L.-C.; Yu, Y.; Zhang, H.; Singh, V.; Zhou, J.; Ehteram, M.; Othman, F.; Yaseen, Z.; et al. *Flood Forecasting Using Machine Learning Methods*; MDPI: Basel, Switzerland, 2019; ISBN 978-3-03897-548-9.
24. Lindersson, S.; Brandimarte, L.; Mård, J.; Di Baldassarre, G. A Review of Freely Accessible Global Datasets for the Study of Floods, Droughts and Their Interactions with Human Societies. *WIREs Water* **2020**, *7*, e1424. https://doi.org/10.1002/wat2.1424.
25. Luís, S.; Freitas, F.E.P.; Rodrigues, N.; Nogueira, A.J.A.; Roseta-Palma, C.; Lima, M.L.; Pinho, L.; Martins, F.C.; Betâmio De Almeida, A.; Cozannet, G.L.; et al. Beliefs on the Local Effects of Climate Change: Causal Attribution of Flooding and Shoreline Retreat. *Revista de Gestão Costeira Integrada* **2017**, *17*, 19–35. https://doi.org/10.5894/rgci-n86.
26. Milfont, T.L.; Evans, L.; Sibley, C.G.; Ries, J.; Cunningham, A. Proximity to Coast Is Linked to Climate Change Belief. *PLoS ONE* **2014**, *9*, e103180. https://doi.org/10.1371/journal.pone.0103180.
27. Neumann, B.; Vafeidis, A.T.; Zimmermann, J.; Nicholls, R.J. Future Coastal Population Growth and Exposure to Sea-Level Rise and Coastal Flooding—A Global Assessment. *PLoS ONE* **2015**, *10*, e0118571. https://doi.org/10.1371/journal.pone.0118571.
28. Elmoustafa, A.M.; Mohamed, M.M. Flash Flood Risk Assessment Using Morphological Parameters in Sinai Peninsula. *Open J. Mod. Hydrol.* **2013**, *3*, 122–129. https://doi.org/10.4236/ojmh.2013.33016.
29. Nguyen, V.; Yariyan, P.; Amiri, M.; Tran, A.; Pham, T.; Do, M.; Ngo, P.; Nhu, V.; Long, N.; Bui, D. A New Modeling Approach for Spatial Prediction of Flash Flood with Biogeography Optimized CHAID Tree Ensemble and Remote Sensing Data. *Remote. Sens.* **2020**, *12*, 1373. https://doi.org/10.3390/rs12091373.
30. Tariq, A.; Yan, J.; Ghaffar, B.; Qin, S.; Mousa, B.G.; Sharifi, A.; Huq, E.; Aslam, M. Flash Flood Susceptibility Assessment and Zonation by Integrating Analytic Hierarchy Process and Frequency Ratio Model with Diverse Spatial Data. *Water* **2022**, *14*, 3069. https://doi.org/10.3390/w14193069.
31. MacManus, K.; Balk, D.; Engin, H.; McGranahan, G.; Inman, R. Estimating Population and Urban Areas at Risk of Coastal Hazards, 1990–2015: How Data Choices Matter. *Earth Syst. Sci. Data Discuss.* **2021**, *13*, 5747–5801. https://doi.org/10.5194/essd-2021-165.

32. Simperler, L.; Kretschmer, F.; Ertl, T. *Analysing the Cause of Urban Pluvial Flooding in a Hillside Settlement*; Springer Verlag: Berlin/Heidelberg, Germany, 2019; pp. 459–463.
33. Olbert, A.I.; Comer, J.; Nash, S.; Hartnett, M. High-Resolution Multi-Scale Modelling of Coastal Flooding Due to Tides, Storm Surges and Rivers Inflows. A Cork City Example. *Coast. Eng.* **2017**, *121*, 278–296. https://doi.org/10.1016/j.coastaleng.2016.12.006.
34. Lewis, M.J.; Palmer, T.; Hashemi, R.; Robins, P.; Saulter, A.; Brown, J.; Lewis, H.; Neill, S. Wave-Tide Interaction Modulates Nearshore Wave Height. *Ocean Dyn.* **2019**, *69*, 367–384. https://doi.org/10.1007/s10236-018-01245-z.
35. Idier, D.; Pedreros, R.; Rohmer, J.; Le Cozannet, G. The Effect of Stochasticity of Waves on Coastal Flood and Its Variations with Sea-Level Rise. *J. Mar. Sci. Eng.* **2020**, *8*, 798. https://doi.org/10.3390/jmse8100798.
36. Gallien, T.W. Validated Coastal Flood Modeling at Imperial Beach, California: Comparing Total Water Level, Empirical and Numerical Overtopping Methodologies. *Coast. Eng.* **2016**, *111*, 95–104. https://doi.org/10.1016/j.coastaleng.2016.01.014.
37. Hughes, M.G.; Moseley, A.S.; Baldock, T.E. Probability Distributions for Wave Runup on Beaches. *Coast. Eng.* **2010**, *57*, 575–584. https://doi.org/10.1016/j.coastaleng.2010.01.001.
38. Chow, A.C.H.; Sun, J. Combining Sea Level Rise Inundation Impacts, Tidal Flooding and Extreme Wind Events along the Abu Dhabi Coastline. *Hydrology* **2022**, *9*, 143. https://doi.org/10.3390/hydrology9080143.
39. Vousdoukas, M.I.; Voukouvalas, E.; Mentaschi, L.; Dottori, F.; Giardino, A.; Bouziotas, D.; Bianchi, A.; Salamon, P.; Feyen, L. Developments in Large-Scale Coastal Flood Hazard Mapping. *Nat. Hazards Earth Syst. Sci.* **2016**, *16*, 1841–1853. https://doi.org/10.5194/nhess-16-1841-2016.
40. Tellman, B.; Sullivan, J.A.; Kuhn, C.; Kettner, A.J.; Doyle, C.S.; Brakenridge, G.R.; Erickson, T.A.; Slayback, D.A. Satellite Imaging Reveals Increased Proportion of Population Exposed to Floods. *Nature* **2021**, *596*, 80–86. https://doi.org/10.1038/s41586-021-03695-w.
41. Kulp, S.A.; Strauss, B.H. New Elevation Data Triple Estimates of Global Vulnerability to Sea-Level Rise and Coastal Flooding. *Nat. Commun.* **2019**, *10*, 4844. https://doi.org/10.1038/s41467-019-12808-z.
42. Gao, S. Geospatial Artificial Intelligence (GeoAI). In *Geography*; Oxford University Press, Oxford, United Kingdom, 2021; ISBN 978-0-19-987400-2.
43. Gao, J.; Pesaresi, M. Downscaling SSP-Consistent Global Spatial Urban Land Projections from 1/8-Degree to 1-Km Resolution 2000–2100. *Sci. Data* **2021**, *8*, 281. https://doi.org/10.1038/s41597-021-01052-0.
44. Cattaneo, A.; Nelson, A.; McMenomy, T. Global Mapping of Urban–Rural Catchment Areas Reveals Unequal Access to Services. *Proc. Natl. Acad. Sci. USA* **2021**, *118*, e2011990118. https://doi.org/10.1073/pnas.2011990118.
45. Friedel, M.J.; Smith, M.E.; Erazo Chica, A.M.; Litke, D. Probable Flood Predictions in Ungauged Coastal Basins of El Salvador. *J. Hydrol. Eng.* **2008**, *13*, 321–332. https://doi.org/10.1061/(ASCE)1084-0699(2008)13:5(321).
46. Godwyn-Paulson, P.; Jonathan, M.P.; Hernandez, F.R.; Muthusankar, G.; Lakshumanan, C. Coastline Variability of Several Latin American Cities alongside Pacific Ocean Due to the Unusual "Sea Swell" Events of 2015. *Environ. Monit Assess* **2020**, *192*, 522. https://doi.org/10.1007/s10661-020-08469-x.
47. Crespin, S.J.; Simonetti, J.A. Loss of Ecosystem Services and the Decapitalization of Nature in El Salvador. *Ecosyst. Serv.* **2016**, *17*, 5–13. https://doi.org/10.1016/j.ecoser.2015.10.020.
48. Porwal, S.; Katiyar, S.K. Performance Evaluation of Various Resampling Techniques on IRS Imagery. In Proceedings of the 2014 Seventh International Conference on Contemporary Computing (IC3), Noida, India, 7–9 August 2014; IEEE: Noida, India, 2014; pp. 489–494.
49. Wu, Z.; Yi, L.; Zhang, G. Uncertainty Analysis of Object Location in Multi-Source Remote Sensing Imagery Classification. *Int. J. Remote Sens.* **2009**, *30*, 5473–5487. https://doi.org/10.1080/01431160903130945.
50. Tan, M.L.; Ficklin, D.L.; Dixon, B.; Ibrahim, A.L.; Yusop, Z.; Chaplot, V. Impacts of DEM Resolution, Source, and Resampling Technique on SWAT-Simulated Streamflow. *Appl. Geogr.* **2015**, *63*, 357–368. https://doi.org/10.1016/j.apgeog.2015.07.014.
51. Lin, B.; Yang, G.; Zhang, Q.; Zhang, G. Semantic Segmentation Network Using Local Relationship Upsampling for Remote Sensing Images. *IEEE Geosci. Remote Sens. Lett.* **2022**, *19*, 8006105. https://doi.org/10.1109/LGRS.2020.3047443.
52. Goshtasby, A.A. Image Resampling and Compositing. In *Image Registration*; Advances in Pattern Recognition; Springer: London, UK, 2012; pp. 401–414, ISBN 978-1-4471-2457-3.
53. Parker, J.A.; Kenyon, R.V.; Troxel, D.E. Comparison of Interpolating Methods for Image Resampling. *IEEE Trans. Med. Imaging* **1983**, *2*, 31–39. https://doi.org/10.1109/TMI.1983.4307610.
54. Gao, X.; Zhang, K.; Tao, D.; Li, X. Image Super-Resolution with Sparse Neighbor Embedding. *IEEE Trans. Image Process.* **2012**, *21*, 3194–3205. https://doi.org/10.1109/TIP.2012.2190080.
55. Zuo, H.; Balmaseda, M.A.; Tietsche, S.; Mogensen, K.; Mayer, M. The ECMWF Operational Ensemble Reanalysis–Analysis System for Ocean and Sea Ice: A Description of the System and Assessment. *Ocean Sci.* **2019**, *15*, 779–808. https://doi.org/10.5194/os-15-779-2019.
56. Apecechea, M.I.; Melet, A.; Armaroli, C. Towards a Pan-European Coastal Flood Awareness System: Skill of Extreme Sea-Level Forecasts from the Copernicus Marine Service. *Front. Mar. Sci.* **2023**, *9*, 1091844. https://doi.org/10.3389/fmars.2022.1091844.
57. Jevrejeva, S.; Williams, J.; Vousdoukas, M.I.; Jackson, L.P. Future Sea Level Rise Dominates Changes in Worst Case Extreme Sea Levels along the Global Coastline by 2100. *Environ. Res. Lett.* **2023**, *18*, 024037. https://doi.org/10.1088/1748-9326/acb504.
58. Mcivor, A.; Spencer, T.; Möller, I.; Spalding, M. *Storm Surge Reduction by Mangroves*; 2012.
59. Gijsman, R.; Horstman, E.M.; van der Wal, D.; Friess, D.A.; Swales, A.; Wijnberg, K.M. *Nature-Based Engineering: A Review on Reducing Coastal Flood Risk with Mangroves*; 2021; Volume 8, ISBN 2296-7745.

60. Narayan, S.; Thomas, C.; Matthewman, J.; Shepard, C.; Geselbracht, L.; Nzerem, K.; Beck, M. *Valuing the Flood Risk Reduction Benefits of Florida's Mangroves*; The Nature Conservancy: Arlington County, VA, USA, 2019.
61. Menéndez, P.; Losada, I.J.; Torres-Ortega, S.; Narayan, S.; Beck, M.W. The Global Flood Protection Benefits of Mangroves. *Sci. Rep.* **2020**, *10*, 4404. https://doi.org/10.1038/s41598-020-61136-6.
62. Zhang, K.; Liu, H.; Li, Y.; Xu, H.; Shen, J.; Rhome, J.; Smith, T.J. The Role of Mangroves in Attenuating Storm Surges. *Estuar. Coast. Shelf Sci.* **2012**, *102–103*, 11–23. https://doi.org/10.1016/j.ecss.2012.02.021.
63. Giri, C.; Ochieng, E.; Tieszen, L.L.; Zhu, Z.; Singh, A.; Loveland, T.; Masek, J.; Duke, N. Status and Distribution of Mangrove Forests of the World Using Earth Observation Satellite Data. *Glob. Ecol. Biogeogr.* **2011**, *20*, 154–159. https://doi.org/10.1111/j.1466-8238.2010.00584.x.
64. He, H.; Garcia, E.A. Learning from Imbalanced Data. *IEEE Trans. Knowl. Data Eng.* **2009**, *21*, 1263–1284. https://doi.org/10.1109/TKDE.2008.239.
65. Akbani, R.; Kwek, S.; Japkowicz, N. *Applying Support Vector Machines to Imbalanced Datasets*; Lecture Notes in Artificial Intelligence (Subseries of Lecture Notes in Computer Science); Boulicaut, J.-F., Esposito, F., Giannotti, F., Pedreschi, D., Eds.; Springer: Berlin/Heidelberg, Germany, 2004; Volume 3201, pp. 39–50.
66. Sadler, J.M.; Goodall, J.L.; Morsy, M.M.; Spencer, K. Modeling Urban Coastal Flood Severity from Crowd-Sourced Flood Reports Using Poisson Regression and Random Forest. *J. Hydrol.* **2018**, *559*, 43–55. https://doi.org/10.1016/j.jhydrol.2018.01.044.
67. Phan, T.-N.; Kappas, M. Comparison of Random Forest, k-Nearest Neighbor, and Support Vector Machine Classifiers for Land Cover Classification Using Sentinel-2 Imagery. *Sensors* **2017**, *18*, 18. https://doi.org/10.3390/s18010018.
68. Huang, Z.; Sang, Y.; Sun, Y.; Lv, J. A Neural Network Learning Algorithm for Highly Imbalanced Data Classification. *Inf. Sci.* **2022**, *612*, 496–513. https://doi.org/10.1016/j.ins.2022.08.074.
69. *IPCC Climate Change 2022: Impacts, Adaptation and Vulnerability. Summary for Policymakers. Working Group II to the Sixth Assessment Report of the Intergovernmental Panel on Climate Change;* H.-O. Pörtner, D.C. Roberts, M. Tignor, E.S. Poloczanska, K. Mintenbeck, A. Alegría, M. Craig, S. Langsdorf, S. Löschke, V. Möller, A. Okem, B. Rama (eds.); Cambridge University Press. Cambridge University Press, Cambridge, UK and New York, NY, USA, 3056; 2022; p. 37.
70. Marconcini, M.; Metz-Marconcini, A.; Üreyen, S.; Palacios-Lopez, D.; Hanke, W.; Bachofer, F.; Zeidler, J.; Esch, T.; Gorelick, N.; Kakarla, A.; et al. Outlining Where Humans Live, the World Settlement Footprint 2015. *Sci. Data* **2020**, *7*, 242. https://doi.org/10.1038/s41597-020-00580-5.
71. Breiman, L. Random Forests. *Mach. Learn.* **2001**, *45*, 5–32. https://doi.org/10.1023/A:1010933404324.
72. Ruckelshaus, M.; Reguero, B.G.; Arkema, K.; Compeán, R.G.; Weekes, K.; Bailey, A.; Silver, J. Harnessing New Data Technologies for Nature-Based Solutions in Assessing and Managing Risk in Coastal Zones. *Int. J. Disaster Risk Reduct.* **2020**, *51*, 101795. https://doi.org/10.1016/j.ijdrr.2020.101795.
73. Reisinger, A.; Garschagen, M.; Mach, K.J.; Pathak, M.; Poloczanska, E.; van Aalst, M.; Ruane, A.C.; Howden, M.; Hurlbert, M.; Mintenbeck, K.; et al. *The Concept of Risk in the IPCC Sixth Assessment Report: A Summary of Cross-Working Group Discussions*; Intergovernmental Panel on Climate Change: Geneva, Switzerland, 2020.
74. Muis, S.; Apecechea, M.I.; Dullaart, J.; De Lima Rego, J.; Madsen, K.S.; Su, J.; Yan, K.; Verlaan, M. A High-Resolution Global Dataset of Extreme Sea Levels, Tides, and Storm Surges, Including Future Projections. *Front. Mar. Sci.* **2020**, *7*, 263. https://doi.org/10.3389/fmars.2020.00263.
75. Rueda, A.; Vitousek, S.; Camus, P.; Tomás, A.; Espejo, A.; Losada, I.J.; Barnard, P.L.; Erikson, L.H.; Ruggiero, P.; Reguero, B.G.; et al. A Global Classification of Coastal Flood Hazard Climates Associated with Large-Scale Oceanographic Forcing. *Sci. Rep.* **2017**, *7*, 5038. https://doi.org/10.1038/s41598-017-05090-w.
76. Luu, C.; Bui, Q.D.; Costache, R.; Nguyen, L.T.; Nguyen, T.T.; Van Phong, T.; Van Le, H.; Pham, B.T. Flood-Prone Area Mapping Using Machine Learning Techniques: A Case Study of Quang Binh Province, Vietnam. *Nat. Hazards* **2021**, *108*, 3229–3251. https://doi.org/10.1007/s11069-021-04821-7.
77. Wang, Z.; Lai, C.; Chen, X.; Yang, B.; Zhao, S.; Bai, X. Flood Hazard Risk Assessment Model Based on Random Forest. *J. Hydrol.* **2015**, *527*, 1130–1141. https://doi.org/10.1016/j.jhydrol.2015.06.008.
78. Solichin, A. Comparison of Decision Tree, Naïve Bayes and K-Nearest Neighbors for Predicting Thesis Graduation. In Proceedings of the 2019 6th International Conference on Electrical Engineering, Computer Science and Informatics (EECSI), Bandung, Indonesia, 18–20 September 2019; pp. 217–222.
79. Mobley, W.; Sebastian, A.; Blessing, R.; Highfield, W.E.; Stearns, L.; Brody, S.D. Quantification of Continuous Flood Hazard Using Random Forest Classification and Flood Insurance Claims at Large Spatial Scales: A Pilot Study in Southeast Texas. *Nat. Hazards Earth Syst. Sci.* **2021**, *21*, 807–822. https://doi.org/10.5194/nhess-21-807-2021.
80. Beccari, B. A Comparative Analysis of Disaster Risk, Vulnerability and Resilience Composite Indicators. *PLoS Curr.* **2016**. https://doi.org/10.1371/currents.dis.453df025e34b682e9737f95070f9b970.
81. Lin, P.-S.S. Building Resilience through Ecosystem Restoration and Community Participation: Post-Disaster Recovery in Coastal Island Communities. *Int. J. Disaster Risk Reduct.* **2019**, *39*, 101249. https://doi.org/10.1016/j.ijdrr.2019.101249.
82. Zennaro, F.; Furlan, E.; Simeoni, C.; Torresan, S.; Aslan, S.; Critto, A.; Marcomini, A. Exploring Machine Learning Potential for Climate Change Risk Assessment. *Earth-Sci. Rev.* **2021**, *220*, 103752. https://doi.org/10.1016/j.earscirev.2021.103752.
83. Yu, Y.-C.; Chen, H.; Shih, H.-J.; Chang, C.-H.; Hsiao, S.-C.; Chen, W.-B.; Chen, Y.-M.; Su, W.-R.; Lin, L.-Y. Assessing the Potential Highest Storm Tide Hazard in Taiwan Based on 40-Year Historical Typhoon Surge Hindcasting. *Atmosphere* **2019**, *10*, 346. https://doi.org/10.3390/atmos10060346.

84. Kirezci, E.; Young, I.R.; Ranasinghe, R.; Muis, S.; Nicholls, R.J.; Lincke, D.; Hinkel, J. Projections of Global-Scale Extreme Sea Levels and Resulting Episodic Coastal Flooding over the 21st Century. *Sci. Rep.* **2020**, *10*, 11629. https://doi.org/10.1038/s41598-020-67736-6.
85. Meinshausen, M.; Nicholls, Z.R.J.; Lewis, J.; Gidden, M.J.; Vogel, E.; Freund, M.; Beyerle, U.; Gessner, C.; Nauels, A.; Bauer, N.; et al. The Shared Socio-Economic Pathway (SSP) Greenhouse Gas Concentrations and Their Extensions to 2500. *Geosci. Model Dev.* **2020**, *13*, 3571–3605. https://doi.org/10.5194/gmd-13-3571-2020.
86. Howard, T.; Palmer, M.D.; Bricheno, L.M. Contributions to 21st Century Projections of Extreme Sea-Level Change around the UK. *Environ. Res. Commun.* **2019**, *1*, 095002. https://doi.org/10.1088/2515-7620/ab42d7.
87. Vousdoukas, M.I.; Mentaschi, L.; Voukouvalas, E.; Verlaan, M.; Jevrejeva, S.; Jackson, L.P.; Feyen, L. Global Probabilistic Projections of Extreme Sea Levels Show Intensification of Coastal Flood Hazard. *Nat. Commun.* **2018**, *9*, 2360. https://doi.org/10.1038/s41467-018-04692-w.
88. López-Dóriga, U.; Jiménez, J.A. Impact of Relative Sea-Level Rise on Low-Lying Coastal Areas of Catalonia, NW Mediterranean, Spain. *Water* **2020**, *12*, 3252. https://doi.org/10.3390/w12113252.